Vibrational characteristics of three-dimensional solids, with applications to earth dams
by Gerald Alvin Frazier

A thesis submitted to the Graduate Faculty in partial fulfillment of the requirements for the degree of DOCTOR OF PHILOSOPHY in Civil Engineering
Montana State University

Abstract:
A concise form of the differential equation of motion for a three-dimensional linearly elastic continuum is developed. To treat this partial differential equation, a three-dimensional finite-element technique is developed, which includes many of the finer points of the method and has a wide range of applicability to media with inhomogeneous and anisotropic properties. A formal solution to the differential equation of motion, including both transient body forces and transient boundary conditions, is presented, which uses the natural modes of vibration.

In preparation for analyzing earth dams for their natural modes of vibration, computer solutions by using both two- and three-dimensional finite-element methods are compared with exact solutions. The lowest four computed natural frequencies of a plane-strain circular cylinder were within 3½% of the exact values, and the lowest radial natural frequency of a free sphere was computed by the three-dimensional finite-element method to within 2½% of the exact value. A hypothetical wedge-shaped dam in a rectangular canyon was analyzed by the three-dimensional method and two non-three-dimensional methods, and the computed vibrational characteristics were compared.

Bouquet Dam and a model of Sannokai Dam, both of which have been tested experimentally, were analyzed by the three-dimensional finite-element method. The lowest three upstream-downstream computed natural frequencies of Bouquet Dam lie from 3.6% to 7.7% below the observed frequencies, while seven of the computed frequencies of the Sannokai Dam model vary from 16% below to 10% above the observed frequencies. The computed mode shapes of the Sannokai model qualitatively agree quite well with the observed shapes. For Bouquet Dam the computed mode shapes follow the observed shapes reasonably well along the crest but considerably overestimate the observed values in the lower regions of the dam. This discrepancy is attributed to an increase in the wave velocities of the actual dam with depth.

The study reveals that there are a multitude of vibration modes of earth dams with frequencies close to the fundamental frequency, and well within the range of frequencies noted in strong motion earthquakes. The existence of these closely spaced frequencies would appear to present serious problems when response calculations are attempted, a fact which should be noted by future investigations.

VIBRATIONAL CHARACTERISTICS OF THREE-DIMENSIONAL SOLIDS, WITH APPLICATIONS TO EARTH DAMS

by

GERALD ALVIN FRAZIER

A thesis submitted to the Graduate Faculty in partial fulfillment of the requirements for the degree

of

DOCTOR OF PHILOSOPHY

in

Civil Engineering

Approved:

Head, Major Department

Chairman, Examining Committee

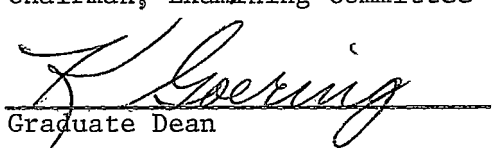

Graduate Dean

MONTANA STATE UNIVERSITY
Bozeman, Montana

August, 1969

ACKNOWLEDGMENTS

The completion of this body of research is a result of the assisting efforts of many individuals to whom the author wishes to extend his sincere appreciation. This three-dimensional investigation is based on many recent advances in the numerical techniques for treating partial differential equations, especially those techniques that utilize the notion of finite elements; consequently, the author wishes to acknowledge those dedicated individuals responsible for improving analysis techniques.

Special gratitude is extended to Professor W. O. Keightley of Montana State University for his guidance and assistance, which were extended freely throughout this investigation. He has been extremely helpful in proof-reading this paper and in offering many helpful suggestions for improving its form. The vibrational studies that Professor Keightley conducted on Bouquet Dam, along with the vibrational studies Professor Okamoto, Dr. Tamura, Dr. Kato, and Dr. Otawa conducted on the agar-agar model of Sannōkai Dam, add very significantly to the value of the author's three-dimensional analytical investigation. The author is very appreciative that these complementary experimental investigations were undertaken.

The author wishes to extend his appreciation to the many individuals who offered technical assistance. The computing center personnel both at Montana State University and at Lawrence Radiation Laboratory helped

considerably with the numerous computing problems that arose. Mr. J. K. Khanna, a fellow graduate student at Montana State University, assisted with this work in a number of ways, just one of which was in providing the author with a plane-strain computer code. Appreciation is also extended to Dr. Glen Martin of Montana State University, to Mr. Michael Gonsior of the Forest Research Laboratory, and to Dr. John Roberts of Lawrence Radiation Laboratory for related discussions that were accompanied by helpful suggestions.

The author wishes to express his sincerest gratitude to his wife for remaining cheerful and harmonious while enduring the role of a graduate student's wife for so many years. She has been actively devoted to the completion of this work by providing her time and services. She conscientiously typed two drafts of this paper, with some assistance from Mrs. Denise McClue. The final draft was typed by Mrs. Margaret Parker, with whom it has been a pleasure to work. The final drafts of the figures, with the exception of Figure 25, were prepared by Mr. Richard McClue.

The computing expenses associated with this investigation were shared by the Department of Civil Engineering and Engineering Mechanics of Montana State University and Lawrence Radiation Laboratory, under a contract (PO-7794903) with Montana State University to study the "Response of Earth Dams to Seismic Motions." The major portion of the

author's support during the tenure of this study was provided by a National Science Foundation Traineeship. Some personal support was also received from Lawrence Radiation Laboratory and Montana State University. Monetary security to alleviate financial crises was provided by Mr. J. A. Frazier, the author's father.

TABLE OF CONTENTS

LIST OF TABLES

LIST OF FIGURES

ABSTRACT

A concise form of the differential equation of motion for a three-dimensional linearly elastic continuum is developed. To treat this partial differential equation, a three-dimensional finite-element technique is developed, which includes many of the finer points of the method and has a wide range of applicability to media with inhomogeneous and anisotropic properties. A formal solution to the differential equation of motion, including both transient body forces and transient boundary conditions, is presented, which uses the natural modes of vibration.

In preparation for analyzing earth dams for their natural modes of vibration, computer solutions by using both two- and three-dimensional finite-element methods are compared with exact solutions. The lowest four computed natural frequencies of a plane-strain circular cylinder were within 3½% of the exact values, and the lowest radial natural frequency of a free sphere was computed by the three-dimensional finite-element method to within 2½% of the exact value. A hypothetical wedge-shaped dam in a rectangular canyon was analyzed by the three-dimensional method and two non-three-dimensional methods, and the computed vibrational characteristics were compared.

Bouquet Dam and a model of Sannōkai Dam, both of which have been tested experimentally, were analyzed by the three-dimensional finite-element method. The lowest three upstream-downstream computed natural frequencies of Bouquet Dam lie from 3.6% to 7.7% below the observed frequencies, while seven of the computed frequencies of the Sannōkai Dam model vary from 16% below to 10% above the observed frequencies. The computed mode shapes of the Sannōkai model qualitatively agree quite well with the observed shapes. For Bouquet Dam the computed mode shapes follow the observed shapes reasonably well along the crest but considerably overestimate the observed values in the lower regions of the dam. This discrepancy is attributed to an increase in the wave velocities of the actual dam with depth.

The study reveals that there are a multitude of vibration modes of earth dams with frequencies close to the fundamental frequency, and well within the range of frequencies noted in strong motion earthquakes. The existence of these closely spaced frequencies would appear to present serious problems when response calculations are attempted, a fact which should be noted by future investigations.

Chapter I

INTRODUCTION

The total failure of a major earth dam today could be catastrophic, and the likelihood of such a disaster increases every year. The number of dams in the world is ever increasing, and frequently new dams are built at relatively poor damsites because the more ideal sites have already been occupied. With the rapid growth of urban areas located in the flood zones of earth dams, the cost to society of a complete failure is ever increasing. In many areas of the country, a single sudden failure would cost society millions of dollars in damages in addition to the loss of many human lives. This problem of the safety of earth dams should be dealt with, and every effort to prevent such a failure should be made.

What effects do earthquakes have on the performance of earth dams? What do past experiences with this problem indicate? Nearly every year a few earth dams somewhere throughout the world experience some earthquake disturbances; yet, with all of this activity only a few major failures have resulted. In fact, the author is aware of only one instance where an earth dam of any size failed to the point that the reservoir could not be retained long enough for a controlled drawdown of the stored water to a safe level. This complete failure of Sheffield Dam, located just north of Santa Barbara, California, is reported, along with a number of less significant failures, by Ambraseys in a survey of earthquake-induced dam failures.[1]

A number of earth dams have suffered considerable damage as a result of earthquakes; yet somehow they remained intact long enough for their reservoirs to be drained.[1,2] However, many related earth structures did not fare as well. Ambraseys cites a number of cases where earth embankments and levees failed completely as a result of earthquake motions. The vulnerability of tailings dams, which are built up of residues from mining operations, to earthquakes is convincingly documented by Dorbry and Alvarez.[3] The extensive damage to tailings dams resulting from the Chilean earthquake of March 28, 1965, indicates the extent to which the properties of the dam fill govern the amount of damage that results from an earthquake. Apparently, the tailings dams have many features that make them susceptible to earthquake damages.

What conditions make one dam more earthquake resistant than another? Certainly, the knowledge of how an earth dam actually behaves during an earthquake would help to answer this question. But the fact is, nobody really understands how an earth dam reacts during an earthquake. Perhaps it will be found that present day construction practices are adequate for the safety of earth dams, but the point is, nobody knows.

One obvious question pertaining to the vibrational behavior of an earth dam is: Are resonant conditions set up in the dam, or does the dam simply follow, without amplifying, the base motions? Evidence is presented by Keightley that the earth dam acts as a bounded linear solid and that

standing waves or modes of vibration actually occur in the dam, at least at very low levels of stress.[4] This evidence had much to do with inspiring this present analytical treatment of the earth dam.

Several factors make the earth dam a particularly challenging problem to treat analytically. First, the boundaries of the dam are irregular, thus placing the problem well beyond the realm of exact mathematics. The dimensions of the dam are generally of the same order of magnitude in all three directions, thereby necessitating the use of a three-dimensional technique. Furthermore, the properties of the dam are not homogeneous, and linearity is representative of the dam's behavior only at low levels of stress.

To date, all attempts to treat the dam analytically have involved gross approximations in both the material properties and the three dimensional shape of the dam. The earliest effort to obtain a mathematical expression for the dynamic behavior of an earth dam appeared in 1936 by Mononobe, Takata, and Matumura.[5] In this early treatment, which was the origin of the shear-wedge method, the geometry of the dam was represented by an infinitely long wedge with a flat bottom. The motions of the wedge are permitted only in the upstream-downstream direction, and these motions result exclusively in shearing distortions so that no relative distortions occur in horizontal lines passing through the thickness of the dam nor in horizontal lines parallel with the crest. Thus the dam is treated as a

vertical shear beam with a linear taper. This shear-wedge representation was extended by Ambraseys[6] to include the effects of vertical end abutments and further extended by Frazier[7] to include the effects of irregular end abutments. These extensions of the method are still restricted to upstream-downstream motions resulting exclusively in shearing distortions.

A different two-dimensional representation of an earth dam was introduced by Ishizaki and Hatakeyama[8] and later analyzed in detail by Chopra and Clough[9]. In these works the geometry of the dam is again represented by an infinitely long wedge with a flat bottom, and no distortions of lines parallel with the crest are permitted; however, general distortions are treated in vertical planes transverse to the axis of the dam. Thus, in this approach, the dam is treated as a plane-strain wedge.

The research in this paper was conducted to improve on the analysis techniques by providing for complete three-dimensional behavior of the earth dam including its irregular geometry. Experimental tests conducted on dam-shaped structures serve to indicate the need for this three-dimensional treatment, and it is these same experimental tests that serve to indicate the degree of success that is achieved by the more generalized treatment.

Chapter II

THE ANALYTICAL APPROACH

II-1 The General Problem

Basically, the vibrating earth dam is a time-dependent boundary-value problem. As with a wide range of physical problems, a solution to a differential equation that governs the behavior of the system within a prescribed region is sought for each instant in time. The mathematical concepts that represent the physical system include the differential equation of motion, the spatial geometry of the region, the boundary conditions to be met at the extremities of the region, the state of the system at the start of the analytical solution, and the time history of the forcing function. In reality the mathematical expression of these five concepts can be very complex, and a completely rigorous solution frequently appears unattainable at the outset. In fact, in the case of the earth dam, compromises to one degree or another must be made in all five of these governing parts to the problem.

Very severe restrictions must usually be imposed on the mathematical representations in order to obtain a solution by classical mathematics. The irregular nature of the boundary geometry alone frequently places the problem well beyond the realm of exact mathematics.

The value of the exact mathematical procedures is not, by any means, lost in this type of analysis. In fact, it frequently appears that the

more complex the physical system, the greater the utility of exact mathematical procedures. For example, it is generally desirable to treat those components of the problem that can be dealt with by exact mathematics at the outset, thereby simplifying the mathematical formulation of the problem. Here, integral transforms are frequently employed effectively. The modified expression thus obtained is then dealt with by approximate mathematics. Even here, however, exact mathematics guide the numerical steps used in achieving a solution.

II-2 Mathematical Representation of a Solid

II-2.1 Equilibrium Equation

The differential equation that governs the mechanical behavior of a three-dimensional solid is included in many texts dealing with continuum mechanics.[10,11] A rather unrestricted derivation of the differential equation follows.

The equilibrium conditions of the arbitrary volume of continuum, pictured on Figure 1, are expressed as follows,

$$\int_V \{B\}\, dV + \int_S \{T\}\, dS = 0. \tag{1}$$

This equation simply expresses that the vector sum of all of the forces acting on a body in equilibrium must be zero. The internal body forces are $\{B\}$, expressed in force per unit volume, and the surface traction

forces are $\{T\}$, expressed in force per unit area. The three components of these column vectors represent forces in the x, y, and z directions, respectively. The cumulative effect of these forces is obtained by integrating over the region where they act: the volume, V, of the solid for the body forces and the surface, S, which encloses the solid for the surface tractions.

The surface tractions $\{T\}$ acting at a point on the surface of V, where the unit outward normal vector is $\{n\}$, are expressed in terms of the general stress tensor as follows,

$$\begin{Bmatrix} T_x \\ T_y \\ T_z \end{Bmatrix} = \begin{bmatrix} \sigma_{xx} & \sigma_{yx} & \sigma_{zx} \\ \sigma_{xy} & \sigma_{yy} & \sigma_{zy} \\ \sigma_{xz} & \sigma_{yz} & \sigma_{zz} \end{bmatrix} \begin{Bmatrix} n_x \\ n_y \\ n_z \end{Bmatrix} \qquad (2,a)$$

or more simply,

$$\{T\} = [\sigma] \{n\} . \qquad (2,b)$$

The components of the unit outward normal vector $\{n\}$ are simply the direction cosines n_x, n_y, and n_z, as expressed in Equation (2,a). An interpretation of the terms of the stress tensor can be obtained from

Figure 2. The condition for equilibrium of moments acting on the infinitesimal body of Figure 2 requires that

$$\sigma_{xy} = \sigma_{yx}$$

$$\sigma_{xz} = \sigma_{zx} \qquad (3)$$

$$\sigma_{yz} = \sigma_{zy}$$

and hence the symmetry of $[\sigma]$

It is noted here that symmetry of the stress tensor of Equation (2) reduces the number of independent stress components from nine to six. These six stress components can be expressed as a two-dimensional matrix of terms as in Equation (2) or as a column of terms,

$$\{\sigma\} = \begin{Bmatrix} \sigma_{xx} \\ \sigma_{yy} \\ \sigma_{zz} \\ \sigma_{xy} \\ \sigma_{xz} \\ \sigma_{yz} \end{Bmatrix} \qquad (4)$$

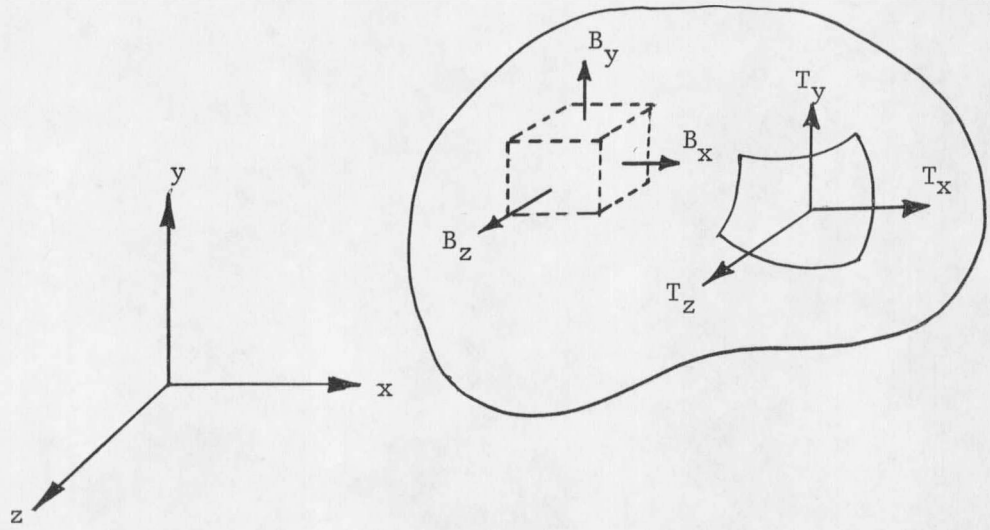

Figure 1. An arbitrary volume, V, of continuum enclosed by the surface, S.

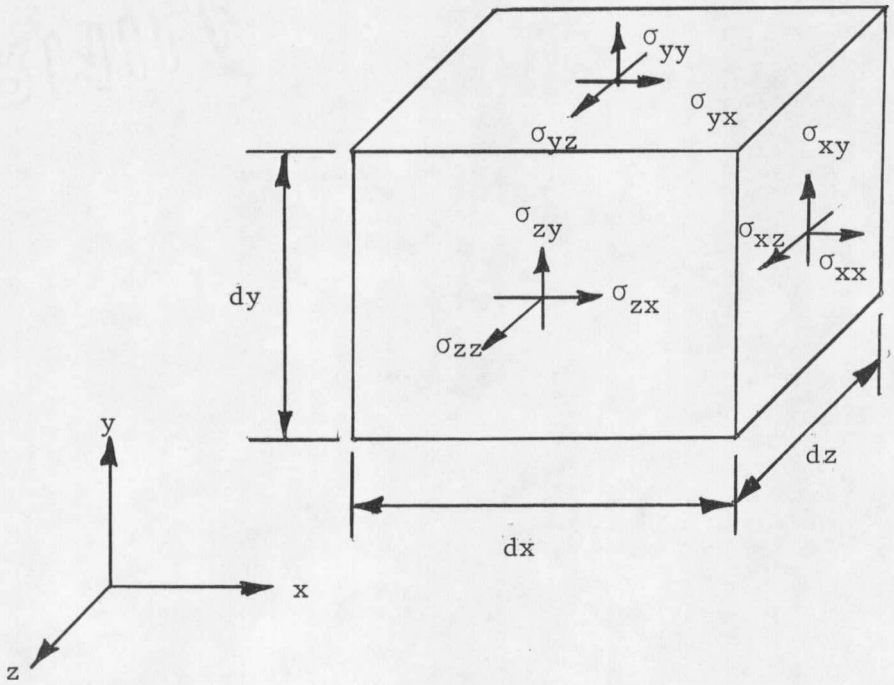

Figure 2. An infinitesimal block of continuum showing the stress components.

This form of expressing the independent stress components is used advantageously in a later section.

{T} from Equation (2,b) is substituted into the surface integral of Equation (1), and Gauss's theorem* [12] is used to obtain the expression

$$\int_V \{\{B\} + <<\Delta>[\sigma]^T\}\}dV = 0. \tag{5}$$

The del operator, operating on $[\sigma]$ is interpreted as

$$<<\Delta>[\sigma]>^T = \begin{Bmatrix} \frac{\partial \sigma_{xx}}{\partial x} + \frac{\partial \sigma_{xy}}{\partial y} + \frac{\partial \sigma_{xz}}{\partial z} \\ \frac{\partial \sigma_{xy}}{\partial x} + \frac{\partial \sigma_{yy}}{\partial y} + \frac{\partial \sigma_{yz}}{\partial z} \\ \frac{\partial \sigma_{xz}}{\partial x} + \frac{\partial \sigma_{yz}}{\partial y} + \frac{\partial \sigma_{zz}}{\partial z} \end{Bmatrix} \tag{6}$$

---

*Gauss's theorem, sometimes referred to as the Divergence Theorem, relates a volume integral and a surface integral as follows,

$$\int_V \nabla \cdot \underset{\rightarrow}{U}\, dV = \int_S \underset{\rightarrow}{n} \cdot \underset{\rightarrow}{U}\, dS$$

where $\underset{\rightarrow}{n}$ is the unit outward normal vector, $\underset{\rightarrow}{U}$ is an arbitrary "smooth" vector function, and V is the volume enclosed by the surface S.

Equation (5) expresses a condition which must be met by a body of a continuum in equilibrium. Because the volume of the continuum is arbitrary, the integrand of Equation (5) must be zero everywhere; hence,

$$\{B\} + \langle\langle\nabla\rangle [\sigma]\rangle^T = 0. \tag{7}$$

Because the interest herein is in dealing with dynamic systems, inertia forces are present. In accordance with d'Alembert's principle* [13], these inertia forces, $-\rho\{\ddot{U}\}$, are treated as body forces and hence as entities of $\{B\}$. Here, ρ represents the mass density, and the three components of the vector $\{\ddot{U}\}$ represent the acceleration components in the x, y, and z directions, respectively. Other body forces that may also be present, for example, weight, are combined into the single term $\{q\}$. Thus, the body forces of Equation (7) are expressed

$$\{B\} = -\rho\{\ddot{U}\} + \{q\}. \tag{8}$$

---

* d'Alembert's principle, a corollary of Newton's second and third laws, provides for treating the inertia forces as body forces. Using d'Alembert's principle the forces acting on a body (including the inertia forces) must sum to zero; whereas, in the approach provided by Newton's laws, the forces acting on a body (excluding the inertia forces) sum to equal the product of the mass and the acceleration of the body.

Replacing {B} in Equation (7) by the terms of Equation (8) gives

$$<<\nabla> [\sigma] >^{T} = \rho\{\ddot{U}\} - \{q\}. \qquad (9)$$

This is the general expression of the equilibrium equation. In this form, however, Equation (9) is of little value for computing features of behavior. To facilitate a solution, the equilibrium equation must be expressed entirely in terms of stress or displacement, but not both.

II-2.2 Simplifications and Approximations

In order to facilitate a solution, the following two simplifications are made:

(1) A linear stress-strain relationship is used to approximate the behavior of the solid, expressed symbolically as follows,

$$\{\sigma\} = [k]\{\varepsilon\} \qquad (10)$$

where $\{\sigma\}$ is a column listing of the six independent stress components given previously by Equation (4), $\{\varepsilon\}$ is a column listing of the six independent strain components,

$$\{\varepsilon\} = \begin{Bmatrix} \varepsilon_x \\ \varepsilon_y \\ \varepsilon_z \\ \varepsilon_{xy} \\ \varepsilon_{xz} \\ \varepsilon_{yz} \end{Bmatrix} \tag{11}$$

and the symmetric six by six matrix [k] contains the elastic constants* of the general anistropic continuum. Equation (10) is frequently referred to as the generalized Hook's law.

Of course, the linear approximation to the stress-strain relationship simplifies the analysis considerably. Of primary consideration here is the fact that the much used principle of superposition can be utilized in the linear analysis.

(2) Although the finite-element method, presented in the following sections of this chapter, is not restricted to homogeneous isotropic media, all work presented herein that involves actual computations deals

---

*The elements of [k] are not actually constant in that they may vary with position in the medium as well as with time and temperature. In this presentation, however, the elements of [k] are assumed to vary with position only, as is the case with an inhomogeneous medium.

exclusively with homogeneous, isotropic media. A more rigorous treatment of the elastic properties of the materials was not attempted, primarily because the degree of refinement to which these material properties are generally measured does not merit a more rigorous treatment.

II-2.3 The Differential Equation of an Elastic Solid

Utilizing the linear stress-strain relationship of Equation (10), the differential equation of motion for an anisotropic solid is expressed in terms of the displacement vector {U}. That is, the equilibrium equation derived in Section II-2.1 is reduced to a form such that the three displacement components are the only dependent variables appearing in Equation (9).

The strain components of Equation (11) are related with the displacements in matrix form as follows,

$$\begin{Bmatrix} \varepsilon_x \\ \varepsilon_y \\ \varepsilon_z \\ \varepsilon_{xy} \\ \varepsilon_{xz} \\ \varepsilon_{yz} \end{Bmatrix} = \begin{bmatrix} \partial/\partial x & 0 & 0 \\ 0 & \partial/\partial y & 0 \\ 0 & 0 & \partial/\partial z \\ \partial/\partial y & \partial/\partial x & 0 \\ \partial/\partial z & 0 & \partial/\partial x \\ 0 & \partial/\partial z & \partial/\partial y \end{bmatrix} \begin{Bmatrix} u \\ v \\ w \end{Bmatrix}, \qquad (12,a)$$

or as expressed in abbreviated form,

$$\{\varepsilon\} = [\mathcal{O}]\{U\}. \tag{12,b}$$

Stress is related to strain by use of the matrix $[k]$ in Equation (10); hence,

$$\{\sigma\} = [k]\,[\mathcal{O}]\,\{U\}. \tag{13}$$

It can be shown that $\langle\nabla\rangle[\sigma]$ of Equation (9) can be expressed as

$$\langle\langle\nabla\rangle[\sigma]\rangle^{T} = [\mathcal{O}]^{T}\{\sigma\} \tag{14}$$

by simply carrying out the indicated operations. By substituting in $\{\sigma\}$ of Equation (13) this expression becomes

$$\langle\langle\nabla\rangle[\sigma]\rangle^{T} = [\mathcal{O}]^{T}[k]\,[\mathcal{O}]\,\{U\}. \tag{15}$$

This relationship is now substituted into Equation (9) to obtain the desired form of the differential equation of motion for an elastic solid,

$$[\mathcal{O}]^{T}[k]\,[\mathcal{O}]\,\{U\} = \rho\{\ddot{U}\} - \{q\}. \tag{16}$$

As indicated previously, the six by six matrix $[k]$ is symmetric, and thereby contains 21 independent elastic "constants" for the case of

the general anisotropic medium. If the medium has one plane of elastic symmetry* [10] it is referred to as monotropic. The number of elastic constants reduces to thirteen for a monotropic medium. For the case of two orthogonal planes of elastic symmetry, the number of independent elastic constants reduces to nine, and the medium is termed orthotropic.

In an isotropic medium the orientation of the coordinate axes has no effect on the matrix [k], and the elements of [k] can be expressed in terms of two independent elastic constants as illustrated in Table I.

---

* Elastic symmetry about a plane exists if the stiffness matrix [k] of Equation (10), based on some x,y,z coordinate axes, is equal to the stiffness matrix [k]' which relates {σ}' and {ε}'. The primed values, {σ}' and {ε}' are based on the x', y', z' coordinate axes which are reflections about the plane of symmetry of the corresponding x,y,z axes. For example, elastic symmetry about the x,y, plane exists if [k] associated with the right-handed coordinate system x,y,z is equal to [k]' associated with the left-handed coordinate system x', y', z' where x'=x, y'=y, and z'=-z. In this special case of a monotropic medium,

$$k_{51}=k_{52}=k_{53}=k_{54}=k_{61}=k_{62}=k_{63}=k_{64}=0$$

as well as the eight corresponding terms located symmetrically in [k].

Table I. The Elastic Constants of an Isotropic Medium

Elements of [k]	Conventional Elastic Constants*					
	G,ν	E,ν	λ,ν	K,ν	λ,G	V_d,V_s
k_{11}, k_{22}, k_{33}	$\frac{2G(1-\nu)}{(1-2\nu)}$	$\frac{E(1-\nu)}{(1+\nu)(1-2\nu)}$	$\frac{\lambda(1-\nu)}{\nu}$	$\frac{3K(1-\nu)}{(1+\nu)}$	$\lambda+2G$	ρV_d^2
k_{44}, k_{55}, k_{66}	G	$\frac{E}{2(1+\nu)}$	$\frac{\lambda(1-2\nu)}{2\nu}$	$\frac{3K(1-2\nu)}{2(1+\nu)}$	G	ρV_s^2
k_{12}, k_{13}, k_{23} k_{21}, k_{31}, k_{32}	$\frac{2G\nu}{(1-2\nu)}$	$\frac{E}{(1+\nu)(1-2\nu)}$	λ	$\frac{3\nu K}{(1+\nu)}$	λ	$\rho(V_d^2 - 2V_s^2)$
all other k_{ij} not appearing above	0	0	0	0	0	0

*

G - Shear Modulus

E - Young's Modulus

λ - Lame's Constant

K - Bulk Modulus

ν - Poison's Ratio

V_d - Dilatational Wave Velocity

V_s - Shear Wave Velocity

II-2.4 The Boundary Conditions

At the extremities of the continuum, conditions are imposed on the dependent variables, $\{U\}$, to make the behavior of the solid conform with its surrounding environment. Boundary conditions encountered in elasticity are generally of the type (i), (ii), or (iii) presented below:

i) Dirichlet conditions, where $\{U\}$ is specified at each point on boundary surface S_i,

$$\{U\} = \{U\}_b \quad \text{on } S_i \ . \tag{17}$$

These boundary conditions occur along the bottom and the end abutments of the dam in cases where the elastic parameters, $[k]$ of Equation (16), of the surrounding canyon are much greater than those of the earth fill. In these cases the displacements $\{U\}_b$ are taken as zero along the dam-canyon interface.

The Dirichlet conditions also occur along moving boundaries where the displacement time history is specified. Seismic disturbances originating away from the dam can be introduced into the analysis by specifying the time history of motion all along the dam-canyon interface in accordance with the disturbance. In this procedure the relative stiffness of the canyon as compared with that of the dam is not relevant.

ii) The generalized Neumann conditions, where the surface tractions $\{T\}_n$ are zero at each point on boundary surface S_{ii}

$$\{T\}_n = 0 \text{ on } S_{ii} \tag{18,a}$$

or by use of Equation (2),

$$[\sigma]\{n\} = 0 \text{ on } S_{ii} \tag{18,b}$$

where $\{n\}$ is a unit outward normal vector to the surface S_{ii}.

The tractions on the surface S_{ii} are expressed in terms of the displacement vector $\{U\}$ by the equation

$$\{T\}_n = [N][k][\partial]\{U\} = 0 \text{ on } S_{ii} \tag{18,c}$$

where $[N]$ relates the surface tractions $\{T\}$ and the stress vector $\{\sigma\}$ of Equation (13) and is defined in terms of the directional cosines,

$$[N] = \begin{bmatrix} n_x & 0 & 0 & n_y & n_z & 0 \\ 0 & n_y & 0 & n_x & 0 & n_z \\ 0 & 0 & n_z & 0 & n_x & n_y \end{bmatrix} \tag{19}$$

These conditions exist along boundary surfaces where the stiffness properties, $[k]$, of the outside continuum are much smaller than those of the dam, as is the case along the air-soil interfaces on the downstream face, the crest, and the upstream face above the water level of the reservoir. Here, on the S_{ii} surfaces, there are essentially no forces acting, and hence the term "free surfaces" is used.

iii) Radiating conditions, where the surface tractions are not zero but are of the form,

$$\{T\} = \{T\}_b + [k]_b \{U\} + [\rho]_b \{\ddot{U}\} \quad \text{on } S_{iii} , \tag{20,a}$$

or expressing $\{T\}$ in terms of $\{U\}$ as in Equation (18,c) gives,

$$[N][k][\partial]\{U\} = \{T\}_b + [k]_b \{U\} + [\rho]_b \{\ddot{U}\} \quad \text{on } S_{iii} , \tag{20,b}$$

where $\{T\}_b$, $[k]_b \{U\}$, and $[\rho]_b \{\ddot{U}\}$ are external sources of traction acting at the boundary.

The externally applied tractions $\{T\}_b$, can be used to represent the water pressure on the upstream face, at least for the static case, when no inertia forces are acting.

The terms $[k]_b \{U\}$ and $[\rho]_b \{\ddot{U}\}$ can be used as a rather crude means for including the static and inertial forces, respectively, that act along elastic boundaries where the stiffness properties $[k]_b$ and the inertial properties $[\rho]_b$ of the outside continuum are of the same order as those of the dam. The boundary conditions for these elastic boundaries, as expressed in Equation (20), do not provide for tractions at one point due to deformations at a different point on S_{iii}, and therefore, the true behavior along these boundaries is being grossly simplified. Both $[k]_b$ and $[\rho]_b$ are restricted to symmetric matrices.

It is of interest here to note that no energy is transferred through boundaries where types (i) or (ii) boundary conditions occur; that is, through boundary surfaces S_i or S_{ii}. This feature has special significance in the finite-element method, presented in a later section of this chapter, in that these boundary conditions are "automatically" provided for in the method, and therefore are referred to as natural boundary conditions.

II-3 Resolving the Space-Dependence

II-3.1 Survey of Methods

As indicated previously, the possibility of locating an exact solution to a boundary-value problem dwindles rapidly as the boundary geometry becomes irregular. Because the primary interest herein is in establishing a procedure for analyzing an earth dam, which, in general, has extremely irregular geometry, it is obvious at the outset that the exclusive use of exact mathematics will severely restrict the analysis. The key to resolving the space-dependence of the differential equation of motion, Equation (16), is the use of a method which deals effectively with irregular boundary geometry.

Two rather general methods for achieving an approximate solution to Equation (16) are cited: 1) a trial-solution type method such as Rayleigh-Ritz's method[13] or Galerkin's method[14], and 2) a zoning type such as the finite-difference method[15] or the finite-element method.[15,16,17]

The procedure of transforming the differential equation into

the complex domain in order to use the powerful theorems of complex variables is not considered here because of its limitation to two-dimensional analysis.[18]

The basic idea behind the trial-solution type method is to assume the form of the solution by selecting functions, without regard to the differential equation, which satisfy the boundary conditions. The approximate solution to the differential equation is then taken as a linear combination of these trial functions. The participation of each function in making up the total solution is determined so as to minimize the error in the differential equation. The mathematical expression that is set up to minimize the factor is what distinguishes one trial-solution type method from another. For example, the well-known Rayleigh-Ritz technique adjusts the participation of the selected functions to minimize the total potential energy of the solid and its load system.

The difficulty of selecting functions which satisfy boundary conditions is a common problem with the trial-solution type method for dealing with solids having boundaries which possess even slight irregularities. This method can be modified to work with functions that satisfy neither the boundary conditions nor the governing differential equation. An example of such a modified method is the Modified Galerkin's Method.[19] The error criterion for determining the participation of each selected function used in these modified methods possesses not only a measure of

the error in the differential equation but also a measure of the degree to which the boundary conditions are met by the combination of the selected functions.

It appears that at best this modification in the trial-solution type method brings certain problems having moderately smooth boundary irregularities within the realm of the method. In order to achieve a good approximate solution by this method, however, the combination of the selected functions must at least roughly satisfy the boundary conditions all along the boundaries, a condition that is generally quite difficult to achieve for irregular boundaries.

A zoning type method provides the best treatment of the irregular boundary geometry. In this type method a gridwork of nodes or isolated reference points is spatially distributed throughout the continuum. Instead of selecting functions defined over the entire bounded continuum, as in the trial-solution type method, functions which are defined only over subregions of the continuum are selected. Usually the functions used in zoning type methods are simply taken as low order polynomials without regard to the differential equation or the boundary conditions. The participation of each of these various functions is then related to the value of displacement at the isolated node points. An approximate solution is obtained by regulating the magnitude of each nodal displacement in an effort to comply with the differential equation and the boundary conditions in some specified manner.

One outstanding feature of this type of method for treating irregular boundary geometry is the manner in which nodal values near the boundaries are adjusted to satisfy the conditions to be met at the boundaries. For treating extremely irregular boundaries, a very fine mesh of nodes, at least in the vicinity of the boundaries, is required. This, of course, can result in a large number of nodal displacements with which to work, but, at least theoretically, the way is clear to deal with such problems.

Until recent years the finite-difference method was by far the most widely used of the zoning type methods. The finite-difference method, as it exists today, has a number of weaknesses which restricts its usage for treating certain problems. For example, the author developed a procedure and wrote a computer code to analyze a three-dimensional earth dam by the finite-difference technique. A rather messy procedure had to be resorted to in order to satisfy the stress boundary conditions along the upstream and downstream faces of the dam, partly because of the skewed relationship between the coordinate axes and the surfaces of the faces, but primarily because, to the author's knowledge, no satisfactory method is available for satisfying stress-type boundary conditions using the finite-difference method. The existing procedures give rise to a system which violates Betti's reciprocal theorem [17,20] in the vicinity of the boundaries where stresses, rather than displacements, are specified. An improved finite-difference procedure which overcomes these difficulties at stress-type boundary conditions is suggested later in this chapter when the finite-element method is developed.

The finite-element method is also a zoning type method, and it is closely akin to the finite-difference method. The basic difference between these two zoning type methods is the manner in which the errors are minimized. In the finite-difference method the differential equation is satisfied exactly at the isolated nodal points; whereas, in the finite-element method an integrated representation of the errors over the entire bounded continuum is minimized. Other differences between the two methods also exist; for example, the displacement functions used in the finite-element method are consistently defined over small element subregions. The displacement functions used in the finite-difference method, on the other hand, are generally defined over subregions that overlap. This results in an inconsistent specification of the displacements at points other than the nodal points.

No difficulty in choosing suitable displacement functions is ever encountered in either zoning type method because low order polynomials are used regardless of the problem. The apriori knowledge of the displacement functions permits a generalized matrix formulation of the entire technique, which in turn, greatly simplifies the problem of programming the technique for a digital computer. The matrix formulation is used effectively in the finite-element method to allow complete freedom in locating the nodal points throughout the bounded continuum. This freedom in the location of the nodal points permits a good geometric fit of irregular boundary geometry without the added necessity of reducing the

zone size in the vicinity of the boundaries. When dealing with stress concentrations, which are associated with near-singularities in the displacement gradients, a smaller zone size can be used near the troublesome areas.

The nodal degrees-of-freedom are adjusted in both the finite-difference method and the finite-element method to minimize errors in both the differential equation and the boundary conditions. In the finite-element method, the boundary conditions are provided for in a way that does not interfere with the systematic treatment of the problem, while at the same time the resulting discrete system is always consistent with Betti's reciprocal theorem. In fact, the boundary conditions are dealt with so easily in the finite-element method that the term "automatic" is frequently used to describe the process for satisfying the boundary conditions.

Additional attractive features of the finite-element method, which makes it even more desirable as an approximate technique, include the relatively simple way in which otherwise complex cases such as inhomogeneous and anisotropic continua are treated. It also appears that convergence conditions can be established and that error bounds can be determined.[15,16]

II-3.2 The Finite-Element Method

Because concern of this section is focussed on the spatial dependence, the problem of dealing explicitly with the time dependence is simply set aside here by performing a Laplace transform on Equation (16) to obtain

$$[\mathcal{O}]^T [k] [\mathcal{O}] \{\overline{U}\} = \rho s^2 \{\overline{U}\} - \rho s\{U(0)\} - \rho\{\dot{U}(0)\} - \{\overline{q}\} \tag{21,a}$$

where $\{\overline{U}\}$ represents the Laplace transform of $\{U\}$, $\{\overline{q}\}$ is the Laplace transform of $\{q\}$, $\{U(0)\}$ and $\{\dot{U}(0)\}$ are the initial values of $\{U\}$ and $\{\dot{U}\}$, respectively, at t=0, and s is the independent variable in the Laplace domain. Upon combining terms, Equation (21,a) is expressed as

$$[\mathcal{O}]^T [k] [\mathcal{O}] \{\overline{U}\} - \rho s^2 \{\overline{U}\} - \{\overline{f}\} = 0 \tag{21,b}$$

where

$$\{\overline{f}\} = - \{\overline{q}\} - \rho s\{U(0)\} - \rho\{\dot{U}(0)\} .$$

Equation (21,b) is expressed in an even more compact form as

$$L\{\overline{U}\} - \{\overline{f}\} = 0 \tag{21,c}$$

by defining the linear spatial operator L as follows,

$$L = [\mathcal{O}]^T [k] [\mathcal{O}] - \rho s^2 [I]$$

where [I] is the 3 by 3 unity matrix having ones along the major diagonal and zeros everywhere else.

In order to obtain the boundary conditions that apply to Equation (21), the boundary conditions of type (i), (ii), and (iii) of Equations (17), (18), and (20), respectively, are transformed into the Laplace domain to obtain the generalized boundary conditions,

$$L_b\{\bar{U}\} = \{\bar{f}\}_b \tag{22}$$

where L_b and $\{\bar{f}\}_b$ are defined according to the governing boundary conditions as follows,

On S_i ,

$$L_b = 1$$

and

$$\{\bar{f}\}_b = \{\bar{U}\}_b ,$$

where $\{\bar{U}\}_b$ is the Laplace transform of $\{U\}_b$.

On S_{ii} ,

$$L_b = [N][k][\partial]$$

and

$$\{\bar{f}\}_b = 0.$$

On S_{iii},

$$L_b = [N][k][\partial] - [k]_b - s^2[\rho]_b$$

and

$$\{\bar{f}\}_b = \{\bar{T}\}_b - s[\rho]_b\{U(0)\} - [\rho]_b\{\dot{U}(0)\} ,$$

where $\{\bar{T}\}_b$ is the Laplace transform of $\{T\}_b$.

The objective of the finite-element method is common to most numerical methods: to approximate the behavior of the continuous system, which can respond in an infinite number of different ways, by a discrete system, which can respond in only a finite number of different ways. Mathematically, the objective is to replace the differential equation of the continuous system, Equation (21,c) and the associated boundary conditions, Equation (22), by a single matrix equation of the form,

$$[K]\{\mathcal{U}\} = \{\overline{F}\} \tag{23}$$

where $[K]$ is a square matrix, generally quite large, which is defined in terms of L and L_b, while $\{\overline{F}\}$ is a column matrix defined in terms of $\{\overline{f}\}$ and $\{\overline{f}\}_b$. Both definitions are specified in accordance with the particular numerical method being employed. The column matrix of unknown coefficients $\{\mathcal{U}\}$ is identified in some way with the dependent variable $\{\overline{U}\}$ of Equation (21,c). Thus, the solution to matrix Equation (23) leads to an approximate solution of $\{\overline{U}\}$. Generally, the larger the matrix equation, that is, the greater the number of coefficients $\{\mathcal{U}\}$, the more refined the approximation in $\{\overline{U}\}$.

The finite degree-of-freedom notion is frequently introduced by restricting the displacement $\{\overline{U}\}$ to a limited function space,

$$\bar{u}(\underset{\rightarrow}{x},s) = \sum_{i=1}^{I} \bar{\alpha}_{u_i}(s)\, p_{u_i}(\underset{\rightarrow}{x})$$

$$\bar{v}(\underset{\rightarrow}{x},s) = \sum_{i=1}^{I} \bar{\alpha}_{v_i}(s)\, p_{v_i}(\underset{\rightarrow}{x})$$

$$\bar{w}(\underset{\rightarrow}{x},s) = \sum_{i=1}^{I} \bar{\alpha}_{w_i}(s)\, p_{w_i}(\underset{\rightarrow}{x}) \qquad (24,a)$$

where $\underset{\rightarrow}{x}$ represents the three-dimensional spatial coordinate vector, $p_{u_i}(\underset{\rightarrow}{x})$, $p_{v_i}(\underset{\rightarrow}{x})$, and $p_{w_i}(\underset{\rightarrow}{x})$ are assumed spatial functions that are combined in a linear fashion according to the participation coefficients $\bar{\alpha}_{u_i}$, $\bar{\alpha}_{v_i}$, and $\bar{\alpha}_{w_i}$ to form the displacement components $\bar{u}$, $\bar{v}$, and $\bar{w}$, respectively. If the functions $p_i(\underset{\rightarrow}{x})$ are members of a complete set, then, in general, the restrictions imposed on $\{\bar{U}\}$ by Equation (24,a) are reduced as I (the number of members of the set) is increased, and, in fact, no restrictions are imposed on $\{\bar{U}\}$ when $I \to \infty$, and the functions form a complete set.

Equation (24,a) is expressed in matrix notation as

$$\{\bar{U}(\underset{\rightarrow}{x},t)\} = [p(\underset{\rightarrow}{x})]\{\bar{\alpha}(s)\} \qquad (24,b)$$

where,

$$[p(\underset{\rightarrow}{x})] = \begin{bmatrix} \langle p_u(\underset{\rightarrow}{x})\rangle & 0 & 0 \\ 0 & \langle p_v(\underset{\rightarrow}{x})\rangle & 0 \\ 0 & 0 & \langle p_w(\underset{\rightarrow}{x})\rangle \end{bmatrix} ,$$

and,

$$\{\overline{\alpha}\ (s)\} = \begin{Bmatrix} \{\overline{\alpha}_u\ (s)\} \\ \{\overline{\alpha}_v\ (s)\} \\ \{\overline{\alpha}_w\ (s)\} \end{Bmatrix} .$$

The general notion of restricting $\{\overline{U}\}$ to a limited function space (Equation (24)) also appears in the finite-element method. However, in the finite-element method $\{\overline{U}\}$ is restricted to a limited function space throughout the domain of each of the many subregions or elements into which the continuum is divided.

The procedure for subdividing the continuum into finite elements is rather arbitrary. Some of the general features that should be considered in this regard are:

1) The number of elements should be sufficiently large to assure good accuracy, yet not so large that the computations become formidable. It is not necessary to fit the boundary geometry of the continuum exactly, but a good fit is certainly desirable.

2) The geometry of each element should be fairly elementary to simplify continuity requirements between elements; triangles and rectangles are popular for two-dimensional analysis. Tetrahedral elements, illustrated in Figure 3, are used for the three-dimensional treatments in this paper. The use of tetrahedral elements for three-dimensional analysis and triangular elements for two-dimensional analyses has certain advantages over elements with square corners for fitting the boundary geometry.

3) The size of the elements can be altered from one region to the next to improve the accuracy. In general, it is desirable that small elements be used in regions where $\{\overline{U}\}$ varies rapidly at the expense of using relatively large elements in regions where $\{\overline{U}\}$ is nearly constant. Also, small elements are frequently necessary near boundaries having irregular geometry to achieve a good geometric fit of the continuum.

Thus, the region is subdivided into a number of finite elements which are then numbered consecutively from one through M, M being the total number of elements. Equation (24) is then applied to each element separately. For example, within the domain of the $m^{\underline{th}}$ element, pictured in Figure 3, the displacement vector $\{\overline{U}\}_m$ is given by

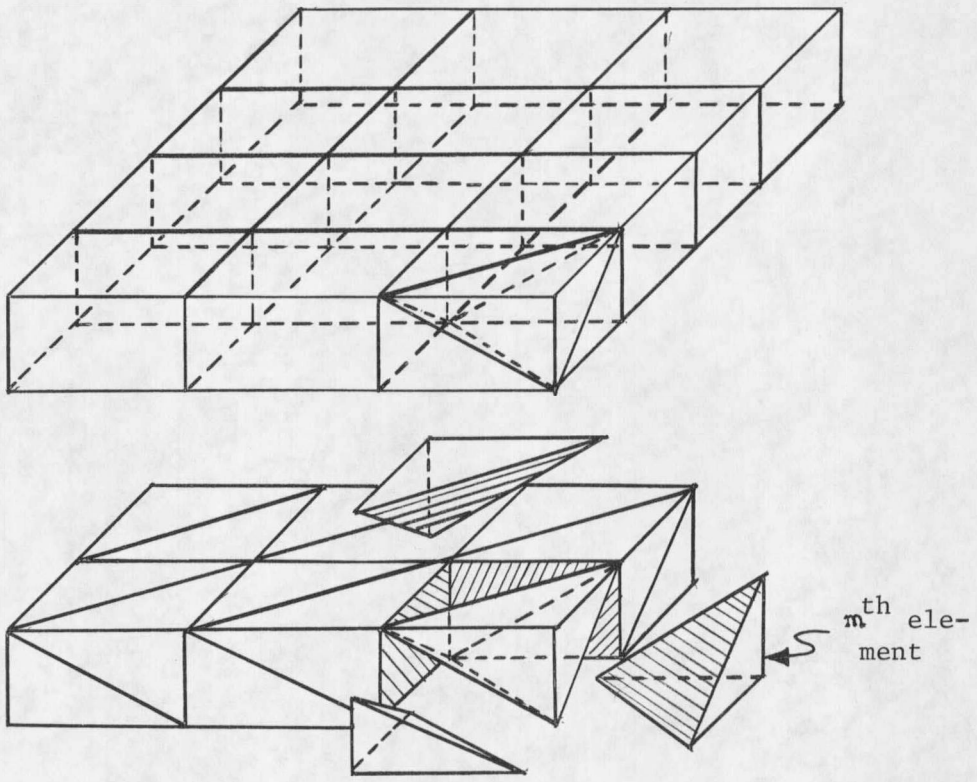

(a) Slab subdivided into tetrahedral elements.

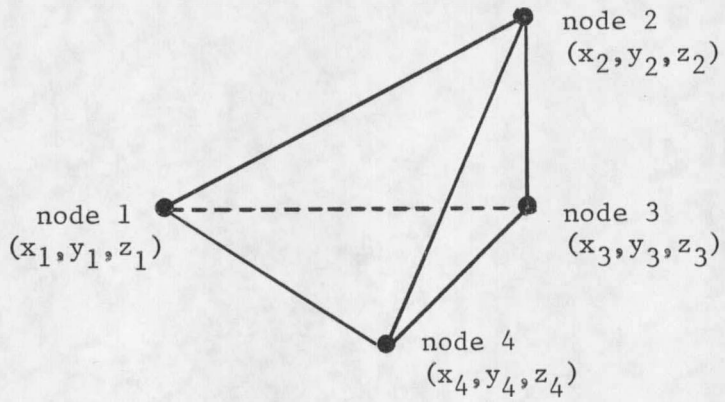

(b) Isolated view of the m^{th} element with nodes at the corners.

Figure 3. Tetrahedral elements.

$$\{\bar{U}(\underset{\rightarrow}{x},s)\}_m = [p(\underset{\rightarrow}{x})]_m \{\bar{\alpha}(s)\}_m \qquad (25)$$

where the subscripted m is used to relate the various terms with the $m^{\underline{th}}$ element.

It becomes apparent that upon defining $\{\bar{U}\}$ over each element of the assemblage according to Equation (25), there is no provision to cause a smooth transition in $\{\bar{U}\}$ from one element to the next. Such a provision must appear in the form of a constraint on the coefficients $\{\bar{\alpha}\}_m$.

In order to deal with this inter-element compatibility problem more directly, the coefficients $\{\bar{\alpha}\}_m$ are replaced by an equal number of new coefficients $\{\bar{\mathcal{U}}\}_m$ where $\{\bar{\mathcal{U}}\}_m$ is a column listing of nodal displacements, which are arranged in groups of three for the tetrahedral element that permits three components of displacement. Each group represents the value of the three-component displacement vector $\{\bar{U}\}_m$ evaluated at an isolated point termed "node", which is located at a strategic point on the outer periphery of the element. Figure 3(b) shows a 4-node tetrahedral element, one node at each corner. Here, in the case of a tetrahedral element, $\{\bar{\mathcal{U}}\}_m$ contains twelve nodal displacements -- three for each of the four nodal points.

Equation (25) is used to relate $\{\bar{\alpha}\}$ and $\{\bar{\mathcal{U}}\}$. If the spatial coordinates of the $j^{\underline{th}}$ nodal point are designated x_j, y_j, z_j, or more concisely, $\underset{\rightarrow}{x}_j$, then, by use of Equation (25),

$$\{\bar{q}(s)\}_m = [P]_m \{\bar{\alpha}(s)\}_m \tag{26}$$

For the case of the four-node tetrahedron of Figure 3(b),

$$[P]_m = \begin{bmatrix} [p(\underset{\rightarrow}{x}_1)]_m \\ [p(\underset{\rightarrow}{x}_2)]_m \\ [p(\underset{\rightarrow}{x}_3)]_m \\ [p(\underset{\rightarrow}{x}_4)]_m \end{bmatrix}$$

In order to complete the transformation from the $\{\bar{\alpha}\}_m$ coordinates to nodal coordinates $\{\bar{q}\}_m$, $[P]_m$ of Equation (26) must be inverted, and therefore the requirement that $[P]_m$ be a square matrix is imposed. $[P]_m$ contains three rows for each nodal point associated with the m^{th} element and three columns for each of the I assumed functions of Equation (24,a). Thus, each of the displacement components, u, v, and w of Equation (24,a) is restricted to one assumed function for each nodal point of the m^{th} element.

Furthermore, two additional conditions necessary for the existence of $[P]_m^{-1}$ are that the assumed functions $[p(\underset{\rightarrow}{x})]_m$ must be independent and the nodal points must be isolated from one another to assure the independence of the nodal values $\{\bar{q}\}_m$. These conditions are not sufficient,

however, as is illustrated by a simple example presented in Appendix A where the above conditions are met, but $[P]_m^{-1}$ does not exist. Another such case occurs on pages 223 and 224 in Reference (6) where an "improved" element is proposed for which $[P]_m^{-1}$ does not exist using standard polynomial terms for $[p(\underset{\rightarrow}{x})]_m$. Those cases where $[P]_m^{-1}$ does not exist are rather rare, and therefore the existence of $[P]_m^{-1}$ can be assumed to exist at this point with little loss of generality.

The desired transformation is achieved by solving Equation (26) for $\{\bar{\alpha}(s)\}_m$ and substituting this expression into Equation (25) to obtain

$$\{\bar{U}(\underset{\rightarrow}{x},s)\}_m = [a(\underset{\rightarrow}{x})]_m \{\bar{q}(s)\}_m \tag{27}$$

where

$$[a(\underset{\rightarrow}{x})]_m = [p(\underset{\rightarrow}{x})]_m [P]_m^{-1} \quad . \tag{28}$$

This equation defines the displacement vector $\{\bar{U}\}$ over the domain of each element of the total assemblage.

The nodal points around the periphery of the elements are located so as to match with the location of the nodal points of adjacent elements. The means of obtaining inter-element compatibility in $\{\bar{U}\}$ is now apparent. The nodal values of $\{\bar{U}\}_m$, termed $\{\bar{q}\}_m$, associated with the $m^{\underline{th}}$ element, are equated to the nodal values in the adjacent elements at the common

nodes. This assures continuity in $\{\overline{U}\}$ across the element interfaces, at least at the nodal points.

This compatibility condition at the nodal points, expressed in matrix form, becomes

$$\{\bar{q}(s)\}_m = [A]_m\{\bar{q}(s)\} \quad . \tag{29}$$

where nodal displacements associated with the $m^{\underline{th}}$ element, $\{\bar{q}\}_m$, represent the local coordinate values and nodal displacements of the combined assemblage of elements, $\{\bar{q}\}$, represent the global coordinate values. The coordinate transformation matrix $[A]_m$ contains information in the form of ones and zeros to relate the local coordinates of the $m^{\underline{th}}$ element with the global coordinates of the combined assemblage.

Thus, it is apparent that this procedure of matching $\{\overline{U}\}$ at the nodal points common to adjacent elements assures continuity in $\{\overline{U}\}$, at least at the nodal points. When $\{\overline{U}\}$ is restricted to linear variations between nodal points, continuity in $\{\overline{U}\}$ is accomplished all along the element interfaces. The four-node tetrahedral element of Figure 3(b) exhibits this desirable feature. Here, as presented in Appendix C, the displacement vector $\{\overline{U}\}$ is restricted to linear variations throughout each tetrahedral element. Therefore, matching the values of $\{\overline{U}\}$ between adjacent elements at the three common nodal points assures continuity in $\{\overline{U}\}$ all along the triangular shaped interfaces.

For reasons that will become apparent later, $\{\bar{\mathcal{U}}(s)\}$ is partitioned to separate the nodal displacements of points located on boundary surfaces S_i, $\{\bar{\mathcal{U}}(s)\}_b$, from all other nodal displacements, $\{\bar{\mathcal{U}}(s)\}_u$,

$$\{\bar{\mathcal{U}}(s)\} = \begin{Bmatrix} \{\bar{\mathcal{U}}(s)\}_u \\ \\ \{\bar{\mathcal{U}}(s)\}_b \end{Bmatrix} . \tag{30}$$

Of course, the nodal displacements $\{\bar{\mathcal{U}}(s)\}_b$ are completely specified by the boundary conditions on S_i; whereas, the remaining 3N (N being the number of unspecified nodal points) nodal displacements $\{\bar{\mathcal{U}}(s)\}_u$ are unspecified, and therefore represent the true number of degrees-of-freedom of the restricted system.

The displacement vector $\{\bar{U}\}$ is expressed in terms of the finite number of global coordinates by substituting $\{\bar{\mathcal{U}}\}_m$ of Equation (29) into Equation (27) to give

$$\{\bar{U}(x,s)\}_m = [a(x)]_m \, [A]_m \{\bar{\mathcal{U}}(s)\} . \tag{31}$$

At the outset it is apparent that, in general, the restricted displacement vector, defined over the domain of each element by Equation (31), cannot satisfy the differential equation and the boundary conditions of the continuum everywhere. Therefore, the problem here is to locate the parti-

cular set of nodal displacements $\{\bar{u}\}$ that in some way minimizes the errors in the system.

One possibility would be to satisfy the differential equation and boundary conditions exactly at as many isolated points as possible. Since $\{\bar{u}\}$ contains three degrees-of-freedom for each nodal point, the differential equation and boundary conditions could be satisfied exactly at each nodal point of the continuum. This procedure would be classified as a consistent finite-difference technique.

In the finite-element method the coefficients $\{\bar{u}\}$ are regulated to minimize a single value, $\bar{J}$ (the bar above the symbol indicates J is expressed in the Laplace domain rather than the time domain), which is used as an index for minimizing the errors in both the differential equation and the boundary conditions. The index $\bar{J}$ is a functional of the dependent variable $\{\bar{U}\}$ of the differential equation as encountered in variational calculus. When the differential equation expresses equilibrium of forces as in Equation (21), the functional $\bar{J}$ represents the Laplace transform of the total potential energy of the system. Thus, in these cases, the requirement for minimum $\bar{J}$ corresponds with the theorem of minimum potential energy.[13]

The extremum expression associated with the differential equation of equilibrium, Equation (21), and the boundary conditions, Equation (22),

of the three-dimensional, anisotropic, inhomogeneous, elastic continuum is,

$$\delta\overline{J} = 0 \ , \tag{32}$$

where

$$\overline{J} = \tfrac{1}{2}\int_V \left(\{ [\mathcal{O}] \{\overline{U}\} \}^T [k] [\mathcal{O}] \{\overline{U}\} + s^2\{\overline{U}\}^T \rho \{\overline{U}\} + 2\{\overline{U}\}^T\{\overline{f}\}\right)dV$$

$$-\tfrac{1}{2}\int_{S_{iii}} \left(\{\overline{U}\}^T [k]_b \{\overline{U}\} + s^2\{\overline{U}\}^T [\rho]_b \{\overline{U}\} + 2\{\overline{U}\}^T\{\overline{f}\}_b\right)dS, \tag{33}$$

and $\delta\overline{J}$ represents all possible infinitesimally small variations in $\overline{J}$ caused by infinitesimally small variations in $\{\overline{U}\}$.

This expression is derived in Appendix B by applying Galerkin's method to Equation (21). The expression can also be written directly from an energy standpoint, the volume integral representing the potential energy of the continuum and the surface integral representing the energy passing through the S_{iii} boundary surface. It is noted that no energy passes through the S_i or the S_{ii} surfaces.

The extremum expression above is entirely equivalent to the boundary value problem expressed by Equation (21) and the associated boundary conditions, Equation (22). Equation (32) merely provides the analyst with a different way of expressing the problem. This fact can be easily verified by applying Euler's theorem[21] to Equation (32) thereby obtaining Equation (21) subjected to the boundary conditions of Equation (22).

Hopefully then, there exist certain features that make the extremum form of expressing the problem more desirable than the equilibrium equation form. One desirable feature of the extremum formulation is that the condition for determining the "best" approximate solution from the restricted displacement space of Equation (31) is apparent. The best solution is simply that for which $\bar{J}$ taken on a minimum value. That is, the unspecified coefficients $\{\bar{u}\}_u$ are located so that,

$$\sum_{n=1}^{3N} \frac{\partial \bar{J}}{\partial \bar{u}_n} = 0 , \tag{34}$$

where the degree-of-freedom number, n, is summed from one to 3N, N being the total number of nodes with unspecified displacements in the assemblage of elements.

Another attractive feature of the extremum formulation is the systematic way in which the boundary conditions are provided for, particularly the natural boundary conditions on boundary surfaces S_i and S_{ii}. Also worth noting in connection with the built-in provision for the boundary conditions is the fact that the coefficients of the resulting force-displacement relationship are always symmetric and positive definite. This fact not only reduces the computational effort of solving the matrix equation but also complies with Betti's reciprocal theorem, discussed previously. It appears that some of the difficulties that the finite-

difference methods have with stress-type boundary conditions could be remedied by working from the extremum formulation of the problem.

Minimizing errors according to the extremum expression of Equation (32) also permits convergence theorems as well as error bounds to be established.[15,16]

In order to use one of the restricted displacement expressions, Equation (27) or Equation (31), to compute $\bar{J}$, the integration of Equation (33) must be performed element by element. $\bar{J}$ is then given by

$$\bar{J} = \sum_{m=1}^{M} \bar{J}_m \tag{35}$$

where

$$\bar{J}_m = \tfrac{1}{2} \int_{V_m} (\{ [\mathcal{O}] \{\bar{U}\}_m \}^T [k] [\mathcal{O}] \{\bar{U}\}_m + s^2 \{\bar{U}\}_m^T \rho \{\bar{U}\}_m + 2\{\bar{U}\}_m^T \{\bar{f}\}) dV$$

$$- \tfrac{1}{2} \int_{S_{iii_m}} (\{\bar{U}\}_m^T [k]_b \{\bar{U}\}_m + s^2 \{\bar{U}\}_m^T [\rho]_b \{\bar{U}\}_m + 2\{\bar{U}\}_m^T \{\bar{f}\}_b) dS \tag{36,a}$$

The assumption that $\bar{J}$ is equal to the sum of the M element contributions $\bar{J}_m$, as in Equation (35), is valid provided the infinitesimal integrals across the element interfaces which are being omitted, make no

contribution to $\bar{J}$. This interface contribution can occur only if the integrand of the volume integral becomes infinite at the element interface. To assure a finite integrand here, $\{\bar{U}\}$ must be continuous across the interfaces. Carrying this argument to the general extremum expression, the next in the volume integral must be continuous across the interfaces to assure a finite integrand.

Substituting $\{\bar{U}\}_m$ of Equation (27) into Equation (36,a) gives,

$$\bar{J}_m = \tfrac{1}{2} \int_{V_m} \{\bar{\mathcal{U}}(s)\}_m^T [b(\underset{\rightarrow}{x})]_m^T [k(\underset{\rightarrow}{x})] [b(\underset{\rightarrow}{x})]_m \{\bar{\mathcal{U}}(s)\}_m \, dV -$$

$$\tfrac{1}{2} \int_{S_{iii_m}} \{\bar{\mathcal{U}}(s)\}_m^T [a(\underset{\rightarrow}{x})]_m [k(\underset{\rightarrow}{x})]_b [a(\underset{\rightarrow}{x})]_m \{\bar{\mathcal{U}}(s)\}_m \, dS +$$

$$\tfrac{1}{2} \int_{V_m} s^2 \{\bar{\mathcal{U}}(s)\}_m^T [a(\underset{\rightarrow}{x})]_m^T \rho(\underset{\rightarrow}{x}) [a(\underset{\rightarrow}{x})]_m \{\bar{\mathcal{U}}(s)\}_m -$$

$$2s \{\bar{\mathcal{U}}(s)\}_m^T [a(\underset{\rightarrow}{x})]^T \rho(\underset{\rightarrow}{x}) [a(\underset{\rightarrow}{x})]_m \{\mathcal{U}(0)\} -$$

$$2\{\bar{\mathcal{U}}(s)\}_m^T [a(\underset{\rightarrow}{x})]_m^T \rho(\underset{\rightarrow}{x}) [a(\underset{\rightarrow}{x})]_m \{\dot{\mathcal{U}}(0)\}_m \, dV -$$

$$\tfrac{1}{2} \int_{S_{iii_m}} s^2 \{\bar{\mathcal{U}}(s)\}_m^T [a(\underset{\rightarrow}{x})]_m [\rho(\underset{\rightarrow}{x})]_b [a(\underset{\rightarrow}{x})]_m \{\bar{\mathcal{U}}(s)\}_m -$$

$$2s\{\bar{\mathcal{U}}(s)\}_m^T [a(\underset{\rightarrow}{x})]_m^T [\rho(\underset{\rightarrow}{x})]_b [a(\underset{\rightarrow}{x})]_m \{\mathcal{U}(0)\}_m -$$

$$2\{\bar{\mathcal{U}}(s)\}_m^T [a(\underset{\rightarrow}{x})]_m^T [\rho(\underset{\rightarrow}{x})]_b [a(\underset{\rightarrow}{x})]_m \{\dot{\mathcal{U}}(0)\}_m \, dS -$$

$$\int_{V_m} \{\bar{u}(s)\}_m^T [a(\vec{x})]_m^T \{\bar{q}(\vec{x},s)\}\, dV -$$

$$\int_{S_{iii_m}} \{\bar{u}(s)\}_m^T [a(\vec{x})]_m^T \{\bar{T}(\vec{x},s)\}_b\, dS \qquad (36,b)$$

where the terms $\{\bar{f}\}$ and $\{\bar{f}\}_b$ have been written in their expanded form, and $[b(\vec{x})]_m = [O][a(\vec{x})]_m$. The terms $\{u(0)\}_m$ and $\{\dot{u}(0)\}_m$ contain the initial displacements and velocities of the nodal points at t=0.

The nodal values $\{\bar{u}(s)\}_m$ are not a function of the spatial coordinates $\vec{x}$ and therefore can be taken outside the integrals. The terms remaining in the various integrals are completely defined at this point; hence, the resulting integration can be carried out to yield the expression

$$\bar{J}_m = \tfrac{1}{2}\{\bar{u}(s)\}_m^T [K]_m \{\bar{u}(s)\}_m + \tfrac{1}{2}s^2\{\bar{u}(s)\}_m^T [M]_m \{\bar{u}(s)\}_m -$$

$$s\{\bar{u}(s)\}_m^T [M]_m \{u(0)\}_m -$$

$$\{\bar{u}(s)\}_m^T [M]_m \{\dot{u}(0)\}_m - \{\bar{u}(s)\}_m^T \{\bar{Q}(s)\}_m \qquad (35,c)$$

where the element "stiffness matrix" is given by

$$[K]_m = \int_{V_m} [b(\underset{\rightarrow}{x})]_m^T [k(\underset{\rightarrow}{x})] [b(\underset{\rightarrow}{x})]_m \, dV -$$

$$\int_{S_{iii_m}} [a(\underset{\rightarrow}{x})]_m^T [k(\underset{\rightarrow}{x})]_b [a(\underset{\rightarrow}{x})]_m \, dS \quad ,$$

the element "mass matrix" is given by

$$[M]_m = \int_{V_m} [a(\underset{\rightarrow}{x})]_m^T \rho(\underset{\rightarrow}{x}) [a(\underset{\rightarrow}{x})]_m \, dV - \int_{S_{iii_m}} [a(\underset{\rightarrow}{x})]_m^T [\rho(\underset{\rightarrow}{x})]_b [a(\underset{\rightarrow}{x})]_m \, dS \quad ,$$

and the element "force matrix" is given by

$$\{\bar{Q}\}_m = \int_{V_m} [a(\underset{\rightarrow}{x})]_m^T \{\bar{q}(\underset{\rightarrow}{x},s)\} dV + \int_{S_{iii_m}} [a(\underset{\rightarrow}{x})]^T \{\bar{T}(\underset{\rightarrow}{x},s)\}_b \, dS \quad .$$

The integrals over the S_{iii_m} surface are nonzero only when the m^{th} element is adjacent to an outside boundary of the continuum where a type (iii) boundary condition exists. The volume integrals are carried out in Appendix C to give the element matrices $[K]_m$ and $[M]_m$ for a generalized four-node tetrahedral element using linear displacement functions.

The local coordinates $\{\bar{u}(s)\}_m$ are expressed in the global coordinates $\{\bar{u}(s)\}$ by use of Equation (29), and the element contributions $\bar{J}_m$ are summed to obtain

$$\bar{J} = \tfrac{1}{2}\{\bar{u}(s)\}^T [K] \{\bar{u}(s)\} + \tfrac{1}{2}s^2\{\bar{u}(s)\}^T [M] \{\bar{u}(s)\} -$$

$$s\{\bar{u}(s)\}^T [M] \{u(0)\} - \{\bar{u}(s)\}^T [M] \{\dot{u}(0)\} - \{\bar{u}(s)\}^T\{\bar{Q}(s)\} \quad \ldots (36,a)$$

where $$[K] = \sum_{m=1}^{M} [A]_m^T [K]_m [A]_m \ ,$$

$$[M] = \sum_{m=1}^{M} [A]_m [M]_m [A]_m \ ,$$

and $$\{\bar{Q}(s)\} = \sum_{m=1}^{M} [A]_m^T \{\bar{Q}(s)\}_m \ .$$

The various matrices are partitioned to separate the specified nodal displacements $\{\bar{u}(s)\}_b$ and the unspecified nodal displacements $\{\bar{u}(s)\}_u$, as in Equation (30),

$$\bar{J} = \tfrac{1}{2} \begin{Bmatrix} \{\bar{u}(s)\}_u \\ \{\bar{u}(s)\}_b \end{Bmatrix}^T \begin{bmatrix} [K]_{uu} & [K]_{ub} \\ [K]_{ub} & [K]_{bb} \end{bmatrix} \begin{Bmatrix} \{\bar{u}(s)\}_u \\ \{\bar{u}(s)\}_b \end{Bmatrix} + \text{(other similarly partitioned matrices).}$$

The index $\bar{J}$ is minimized with respect to the degrees-of-freedom $\{\bar{q}(s)\}_u$ by setting the partial derivatives of Equation (34) equal to zero to obtain the expression,

$$\frac{\partial \bar{J}}{\partial \{\bar{q}(s)\}_u} = 0 = [K]_{uu}\{\bar{q}(s)\}_u + [K]_{ub}\{\bar{q}(s)\}_b +$$

$$s^2[M]_{uu}\{\bar{q}(s)\}_u +$$

$$s^2[M]_{ub}\{\bar{q}(s)\}_b -$$

$$s[M]_{uu}\{q(0)\}_u - s[M]_{ub}\{q(0)\}_b -$$

$$[M]_{uu}\{\dot{q}(0)\}_u - [M]_{ub}\{\dot{q}(0)\}_b - \{\bar{Q}(s)\}_u \quad . \quad . \quad . \quad . \quad (37)$$

This expression utilizes the symmetry in $[K]$ and $[M]$.

The matrix equation above is transformed back into the time domain by performing an inverse Laplace transform to obtain

$$[M]_{uu}\{\ddot{q}(t)\}_u + [K]_{uu}\{q(t)\}_u = \{F(t)\} \qquad (38)$$

where

$$\{F(t)\} = + \{Q(t)\}_u - [K]_{ub}\{q(t)\}_b - [M]_{ub}\{\ddot{q}(t)\}_b \quad .$$

Thus, the finite-element method transforms the time and spatial dependent partial differential Equation (16), and the associated boundary conditions into an ordinary, matrix, differential equation in time. The dependent variable of the partial differential equation, $\{U(\underset{\rightarrow}{x},t)\}$, is related to the column matrix of nodal displacements, $\{\mathcal{U}(t)\}_u$, through the matrices $[a(\underset{\rightarrow}{x})]_m$ and $[A]_m$ of Equation (31),

$$\{U(\underset{\rightarrow}{x},t)\}_m = [a(\underset{\rightarrow}{x})]_m [A]_m \begin{Bmatrix} \{\mathcal{U}(t)\}_u \\ \{\mathcal{U}(t)\}_b \end{Bmatrix} , \tag{39}$$

and the stresses in the continuum are given by

$$\begin{aligned} \{\sigma(\underset{\rightarrow}{x},t)\}_m &= [k(\underset{\rightarrow}{x})]\ [\mathcal{O}]\ [a(\underset{\rightarrow}{x})]_m [A]_m \begin{Bmatrix} \{\mathcal{U}(t)\}_u \\ \{\mathcal{U}(t)\}_b \end{Bmatrix} \\ &= [k(\underset{\rightarrow}{x})]\ [b(\underset{\rightarrow}{x})]_m [A]_m \begin{Bmatrix} \{\mathcal{U}(t)\}_u \\ \{\mathcal{U}(t)\}_b \end{Bmatrix} . \end{aligned} \tag{40}$$

II-4 Resolving the Time Dependence

The second order differential equation in time that is to be solved, Equation (38), has no provision for energy dissipation. If the forcing function $\{F(t)\}$ goes to zero after exciting motions in the continuum, the continuum will continue to vibrate indefinitely. This behavior is contrary to reality; therefore, exponential damping is introduced in the form of a velocity dependent term. Equation (38) then becomes,

$$[M]_{uu}\{\ddot{q}(t)\}_u + [C]_{uu}\{\dot{q}(t)\}_u + [K]_{uu}\{q(t)\} = \{F(t)\} \quad . \quad (41)$$

The elements in $[C]_{uu}$ are to be assigned to cause computed behavior to appear as observed physical behavior. There are not actually $(3N)^2$ such coefficients to be assigned, however, because of the restrictions placed on $[C]_{uu}$, namely that $[C]_{uu}$ must become a diagonal matrix under the same similarity transformation that causes $[M]_{uu}$ and $[K]_{uu}$ to become diagonal. This requirement results in 3N coefficients to be determined experimentally, one for each natural mode of vibration of the discrete system. This form of damping is called modal damping.[17]

When dealing with seismic disturbances, the forcing function $\{F\}$ has an irregular time history, and therefore, numerical methods must be employed for solving Equation (41). One approach would be to step the

solution numerically over brief time intervals starting with the initial conditions $\{\mathcal{U}(0)\}$ and $\{\dot{\mathcal{U}}(0)\}$ evaluated at t=0. In general, this stepping procedure from time t_i to t_{i+1} can be accomplished by use of two steps: (1) Knowing $\{\mathcal{U}_i\}$ and $\{\dot{\mathcal{U}}_i\}$, $\{\ddot{\mathcal{U}}_i\}$ is obtained from the governing differential equation, and then (2) $\{\mathcal{U}_{i+1}\}$ and $\{\dot{\mathcal{U}}_{i+1}\}$, evaluated at t_{i+1}, are extrapolated from $\{\mathcal{U}_i\}$, $\{\dot{\mathcal{U}}_i\}$, and $\{\ddot{\mathcal{U}}_i\}$ by means of a Taylor series expansion. Such a procedure is not restricted to constant coefficients $[M]_{uu}$, $[C]_{uu}$, and $[K]_{uu}$, and therefore is suited for treating nonlinear problems.

This paper is concerned exclusively with linear behavior. Thus, the solution to Equation (41) can be obtained by superimposing the response of the individual modes of vibration. That is,

$$\{\mathcal{U}(t)\}_u = \sum_{n=1}^{3N} T_n(t)\{\Phi\}_n$$

$$= [\Phi]\{T(t)\} \tag{42}$$

where 3N is the number of degrees-of-freedom (N being the number of unspecified nodal points), $T_n(t)$ is the time dependent participation factor of the $n^{\underline{th}}$ mode $\{\Phi\}_n$.

The modes of vibration $\{\Phi\}_n$ and their associated natural frequencies ω_n are defined by the eigenvalue expression

$$[K]_{uu}\{\Phi\}_n = \omega_n^2 [M]_{uu}\{\Phi\}_n \ , \tag{43}$$

or including all the modes and frequencies in a single equation,

$$[K]_{uu}[\Phi] = [M]_{uu}[\Phi]\lceil\Omega^2\rfloor \tag{44}$$

where $\lceil\Omega^2\rfloor$ is a diagonal matrix of eigenvalues, ω_n^2 . Physically, $[\Phi]$ and $\lceil\Omega^2\rfloor$ represent an approximation to the mode shapes and natural frequencies squared of the continuum with the specified boundary displacements $\{U\}_b$ along S_i set to zero.

A more standard form of the eigenvalue expression is obtained by expressing $[M]_{uu}$ as the product of the lower triangular matrix $[L]$ and the upper triangular matrix $[L]^T$,

$$[M]_{uu} = [L][L]^T \ , \tag{45}$$

and then by performing the coordinate transformation,

$$[X] = [L]^T[\Phi] \ . \tag{46}$$

Substituting Equations (45) and (46) into Equation (44) then premultiplying by $[L]^{-1}$ gives

$$[A][X] = [X]\lceil\Omega^2\rfloor \tag{47}$$

where

$$[A] = [L]^{-1}[K]_{uu}[L]^{T-1} .$$

The eigenvalues $\lceil\Omega^2\rfloor$ and the eigenvectors $[X]$ are computed from Equation (47) using standard techniques.[22] Clearly, the so-called generalized mass matrix, expressed as

$$\lceil m\rfloor = [X]^T[X], \tag{48,a}$$

or incorporating Equation (46) as

$$\lceil m\rfloor = [\Phi]^T[M]_{uu}[\Phi] , \tag{48,b}$$

is a diagonal matrix. This fact is shown by premultiplying Equation (47) by $[X]^T$ to obtain

$$[X]^T[A][X] = [X]^T[X]\lceil\Omega^2\rfloor , \tag{49,a}$$

then transposing each side to obtain

$$[X]^T[A][X] = [\Omega^2][X]^T[X] \tag{49,b}$$

since $[A]$ and $[\Omega^2]$ are symmetric.

Equation (49,b) is subtracted from (49,a) and the products $[X]^T[X]$ are replaced by $[\mathcal{M}]$ to obtain the expression

$$[\mathcal{M}][\Omega^2] - [\Omega^2][\mathcal{M}] = 0 \, . \tag{50}$$

The left hand side is zero term by term, therefore,

$$\mathcal{M}_{ij}(\omega_j^2 - \omega_i^2) = 0 \, . \tag{51}$$

With the exception of degenerate frequencies, $\omega_j^2 \neq \omega_i^2$, therefore, $\mathcal{M}_{ij} = 0$ for $i \neq j$. When degenerate frequencies are encountered, the associated eigenvectors $\{X\}_i$ and $\{X\}_j$ can be made orthogonal, and therefore, taking $[\mathcal{M}]$ as a diagonal matrix results in no loss of generality.

Premultiplying Equation (44) by $[\Phi]^T$ it is seen that the generalized stiffness matrix,

$$[\mathcal{K}] = [\Phi]^T[K]_{uu}[\Phi] \, , \tag{52,a}$$

$$[\mathcal{K}] = [\mathcal{M}][\Omega^2] \tag{52,b}$$

is also a diagonal matrix.

Thus, Equations (48,b) and (52) represent the similarity transformations that diagonalize $[M]_{uu}$ and $[K]_{uu}$, respectively. To facilitate the solution, the requirement that $[C]_{uu}$ is also diagonalized by this transformation is made, that is,

$$\lceil \mathcal{C} \rfloor = [\Phi]^T [C]_{uu} [\Phi] \quad . \tag{53,a}$$

Here $\lceil \mathcal{C} \rfloor$ is a diagonal matrix that can be expressed as

$$\lceil \mathcal{C} \rfloor = 2 \lceil \mathcal{M} \rfloor \lceil \zeta \rfloor \lceil \Omega \rfloor \tag{53,b}$$

without loss of generality.

The n^{th} element of the diagonal matrix $\lceil \zeta \rfloor$ is interpreted as the ratio of the effective damping of the n^{th} mode $\{\Phi\}_n$ to the critical damping. These damping ratios $\lceil \zeta \rfloor$ are to be determined experimentally. For example, Keightley[4] conducted vibrational tests on an earth dam and measured damping ratios from about .03 to .06 for the lowest few modes of vibration. These values are of course strongly dependent upon the magnitude of the motions.

The nodal displacements $\{\mathcal{U}(t)\}_u$ of Equation (41) are taken as a linear combination of the modes at each instant in time as expressed in Equation (42) to yield,

$$[M]_{uu}[\Phi]\{\ddot{T}(t)\} + [C]_{uu}[\Phi]\{\dot{T}(t)\} + [K]_{uu}[\Phi]\{T(t)\} = \{F(t)\} \quad . \quad . \quad . \quad (54)$$

This set of interdependent equations are decoupled by simply premultiplying by $[\Phi]^T$ to obtain,

$$[\mathcal{M}]\{\ddot{T}(t)\} + 2[\mathcal{M}][\zeta][\Omega]\{\dot{T}(t)\} + [\mathcal{M}][\Omega^2]\{T(t)\} = [\Phi]^T\{F(t)\} \quad , \quad . \quad . \quad . \quad (55)$$

where Equations (48,b), (52,a), (52,b), (53,a), and (53,b) were employed. Equation (55) is premultiplied by $[\mathcal{M}]^{-1}$ to obtain,

$$\{\ddot{T}(t)\} + 2[\zeta][\Omega]\{\dot{T}(t)\} + [\Omega^2]\{T(t)\} = [\mathcal{M}]^{-1}[\Phi]^T\{F(t)\} \quad . \quad . \quad . \quad (56)$$

Each of the decoupled equations represented above is treated separately. The irregular nature of the forcing function is effectively dealt with by Duhamel's convolution integral,[23] which convolves the impulse response of the left side of Equation (56) with the forcing function appearing on the right. The solution to the n^{th} equation satisfying the initial conditions, $T_n(0)$ and $\dot{T}_n(0)$, is

$$T_n(t) = \frac{e^{-\zeta_n \omega_n t}}{\omega_{dn}} \left(\zeta_n \omega_n T_n(0) + \dot{T}_n(0)\right) \sin(\omega_{dn} t) +$$

$$\omega_{dn} T_n(0) \cos(\omega_{dn} t) +$$

$$\frac{1}{\omega_{dn} \mathcal{M}_{n,n}} \int_0^t e^{-\zeta_n \omega_n (t-\tau)} \sin \omega_{dn}(t-\tau) \{\Phi\}^T_n \{F(\tau)\} d\tau \quad , \qquad (57)$$

where ω_{dn} is the damped natural frequency,

$$\omega_{dn} = \omega_n \sqrt{1 - \zeta^2} \qquad (58)$$

The solution for the combined set of participation factors $\{T(t)\}$ is expressed in matrix form as,

$$\{T(t)\} = \lceil \Omega_d \rfloor^{-1} \lceil e^{-\zeta\omega t} \rfloor \lceil \sin \omega_d t \rfloor \{ \lceil \zeta \rfloor \lceil \Omega \rfloor \{T(0)\} + \{\dot{T}(0)\} \} +$$

$$\lceil e^{-\zeta\omega t} \rfloor \lceil \cos \omega_d t \rfloor \{T(0)\} +$$

$$\lceil \Omega_d \rfloor^{-1} \lceil \mathcal{M} \rfloor^{-1} \int_0^t \lceil e^{-\zeta\omega(t-\tau)} \rfloor \lceil \sin \omega_d (t-\tau) \rfloor [\Phi]^T \{F(\tau)\} d\tau \qquad (59)$$

in which the symbols $\lceil \ \rfloor$ enclosing the various functions indicate a diagonal listing of the enclosed functions evaluated at $n = 1, 2, \ldots 3N$.

The initial conditions, $\{T(0)\}$ and $\{\dot{T}(0)\}$ are expressed in terms of the initial nodal values $\{\mathcal{U}(0)\}$ and $\{\dot{\mathcal{U}}(0)\}$ by use of Equation (42),

$$\{T(0)\} = [\Phi]^{-1}\{\mathcal{U}(0)\}_u$$

$$\{\dot{T}(0)\} = [\Phi]^{-1}\{\dot{\mathcal{U}}(0)\}_u \quad . \tag{60}$$

Substituting $\{T(t)\}$ from Equation (59) into Equation (42) and utilizing Equation (60) above gives the desired expression for the nodal displacements at any time, t, in terms of the seismic forcing function $\{F(t)\}$, and the initial conditions $\{\mathcal{U}(0)\}_u$ and $\{\dot{\mathcal{U}}(0)\}_u$,

$$\{\mathcal{U}(t)\}_u = [\Omega_d]^{-1}\left[e^{-\zeta\omega t}\right]\left[\sin \omega_d t\right]\{[\zeta][\Omega]\{\mathcal{U}(0)\} + \{\dot{\mathcal{U}}(0)\}\} +$$

$$\left[e^{-\zeta\omega t}\right]\left[\cos \omega_d t\right]\{\mathcal{U}(0)\} +$$

$$[\Phi][\Omega_d]^{-1}[\mathcal{M}]^{-1}\int_0^t \left[e^{-\zeta\omega(t-\tau)}\right]\left[\sin \omega_d (t-\tau)\right][\Phi]^T\{F(\tau)\}d\tau \quad .$$

. . . (61)

Chapter III

TEST CALCULATIONS USING THE FINITE-ELEMENT METHOD

III-1 Plane-Strain Analysis

III-1.1 Plane-Strain Finite-Element Computer Code Using Triangular Elements

A computer code was programmed by Mr. J. K. Khanna, a graduate student in Civil Engineering at Montana State University, to compute the natural frequencies and mode shapes of a solid restricted to plane-strain motions. This two-dimensional analysis is carried out using the finite-element method with simple triangular elements that provide for linear variations in displacement. This particular finite-element scheme is widely used, and it is described in References 16 and 17.

The mass matrix, $[M]_{uu}$ of Equation (43), used in this computer code is generated from a lumped-mass system, and hence is a diagonal matrix. Each diagonal element of the mass matrix represents the mass in the region of a nodal point. For example, m_{ii} represents the mass in the region of the node associated with the i^{th} displacement. Although, in general, there is some arbitrariness in regard to the magnitude of the mass at each node, this computer code takes the mass at each node to be equal to one-third the mass of the triangle elements joining at the node. It is noted that the term mass is used here as mass per unit thickness transverse to the plane of the strain.

The natural frequencies squared and modes of vibration of the plane-strain continuum are then approximated numerically by the eigenvalues and eigenvectors, respectively, of the matrix equation,

$$[K]_{uu}\{\Phi\}_n = \omega_n^2 [M]_{uu} \{\Phi\}_n \tag{62}$$

The eigenvalues and eigenvectors are computed in the plane-strain code using Jacobi's method[22].

III-1.2 The Vibrational Characteristics of a Plane-Strain Circular Cylinder Using Triangular Elements

In order to validate the plane-strain code and to gain some experience with the approximations involved in the finite-element method, a plane-strain solid for which the exact natural frequencies and mode shapes are available was analyzed numerically, and the results are compared with the exact solutions. Although the need for such a comparison is of unquestionable importance, surprisingly few finite-element results have been compared with exact solutions in the finite-element literature. In fact, no such comparison for the vibrational characteristics of a plane-strain solid has been made previously, to the writer's knowledge.

Due to the extremely elementary boundary conditions and boundary geometry associated with the infinitely long, solid, elastic circular cylinder having rigid boundaries (zero displacement at r=a in Figure 4), the

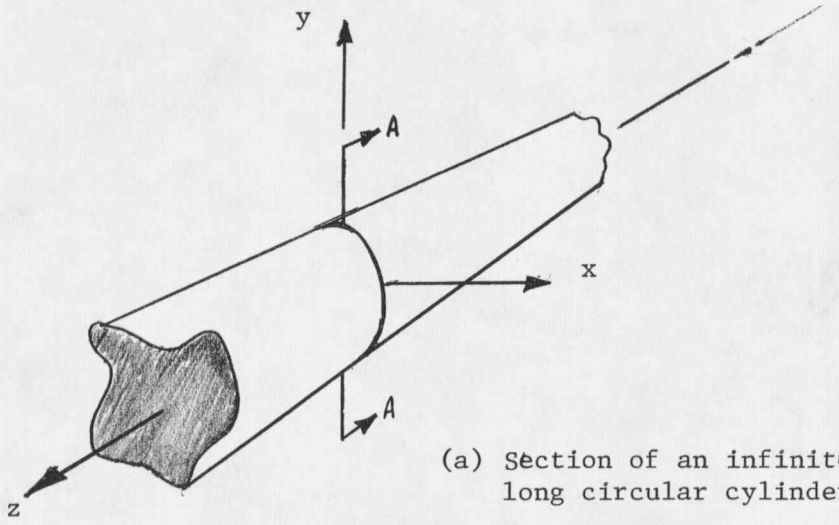

(a) Section of an infinitely long circular cylinder.

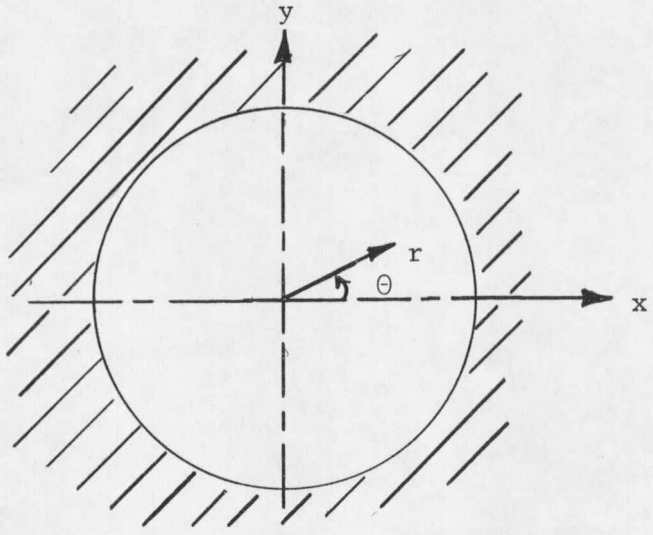

(b) Circular cross-section A-A with rigid boundaries at r=a.

Figure 4. Infinitely long circular-cylinder with rigid boundaries at r = a.

exact natural frequencies and mode shapes for free transverse vibrations can be obtained. Those characteristic solutions where the mode shapes vary sinusoidally with the angular coordinate Θ are derived in Reference 24, and those characteristic solutions where the mode shapes are independent of Θ, which are omitted in Reference 24, are derived in Appendix D.

Figure 5 shows five assemblages of triangular elements that represent a circular cross-section to various degrees of refinement. The characteristic frequencies and modes were computed for each assemblage pictured. Four of the computed frequencies that are associated with rather basic modes of vibration are compared with the corresponding exact frequencies in Figure 6 through the use of the dimensionless frequency, $\Omega = \frac{\omega a}{V_s}$, where ω is the circular frequency, a is the outer radius of the circular cross-section, and V_s is the shear wave velocity. Also included in Figure 6 is a sketch of each of the five mode shapes whose frequencies are being compared.

Only one natural mode of vibration appears in the 1-node assemblage of Figure 5(a): the one in which the center of the circular cross-section vibrates along a major diagonal. Additional natural modes of vibration appear in the more refined assemblages. As the element configuration is refined, Figure 6 shows a pronounced trend for the numerically computed natural frequencies to approach the exact frequencies.

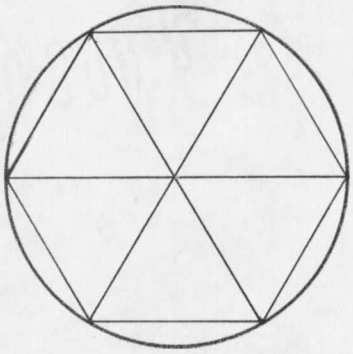

(a) 1-node assemblage

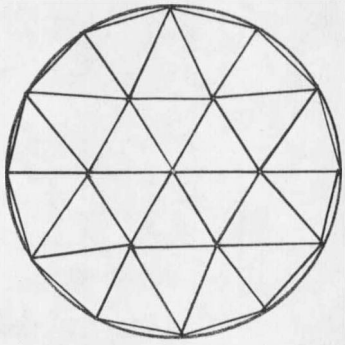

(b) 7-node assemblage

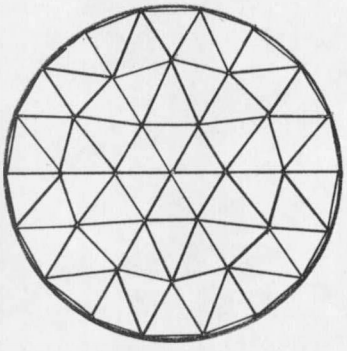

(c) 19-node assemblage

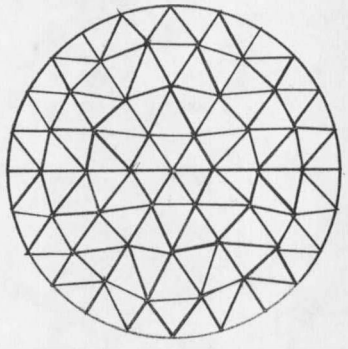

(c) 37-node assemblage

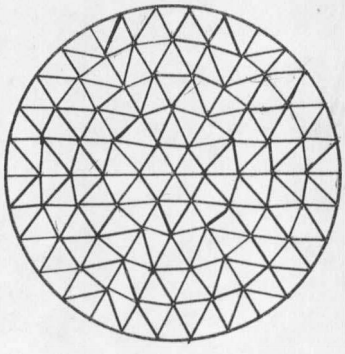

(e) 61-node assemblage

Figure 5. Assemblages of triangular elements representing a circular cross-section of radius "a" of an infinitely long cylinder.

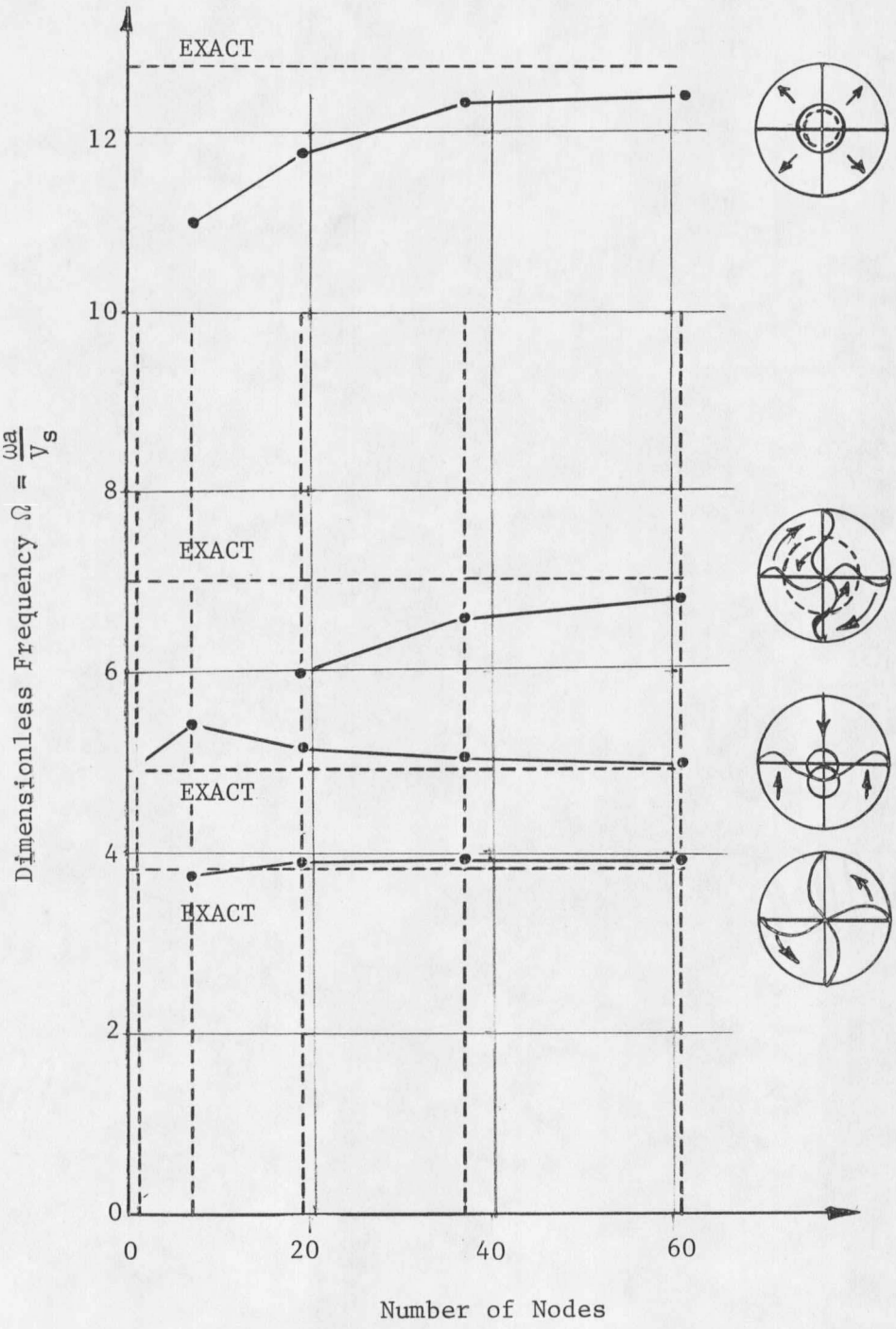

Figure 6. Numerically computed natural frequencies using five different element refinements compared with the exact frequencies for the infinitely long circular-cylinder ($\nu = 0.45$).

The four numerically computed natural frequencies pictured in Figure 6 are all within 3½% of exact frequencies using the 61-node assemblage of Figure 5(e).

III-2 Three-Dimensional Analysis

III-2.1 Three-Dimensional Finite-Element Computer Code Using Tetrahedral Elements

A computer code was programmed by the author to generate the two matrices $[K]_{uu}$ and $[M]_{uu}$ of Equation (43) for a three-dimensional assemblage of tetrahedral elements. The element stiffness matrix $[K]_m$*, used in the code, is defined in terms of the tetrahedral geometry and properties by Equation (C-18) of Appendix C. Just as in the plane-strain analysis, the displacements over the region of an element are restricted to uniform and linearly varying displacement functions. Thus, each tetrahedral element has twelve degrees-of-freedom: one uniform displacement function and three linearly varying displacement functions for each of the three components of displacement, u, v, and w.

The distributed mass of the continuum is approximated by lumped masses at the nodal points of the element assemblage, and hence, $[M]_{uu}$

---

* $[K]_m$ is used to generate the stiffness matrix of the assemblage of elements, $[K]$, according to Equation (36).

is again a diagonal matrix just as in the plane-strain analysis. The quantitative values of the various nodal masses are provided by the analyst as input data to the computer code. The distributed mass matrix, derived in Appendix C, is a different scheme for defining $[M]_{uu}$ not used in this computer analysis, which would not burden the analyst with the job of assigning the elements to the mass matrix.

Following the generation of the two matrices $[K]_{uu}$ and $[M]_{uu}$, the algebraic eigenvalue problem of Equation (43),

$$[K]_{uu} \{\Phi\}_n = \omega_n^2 [M]_{uu} \{\Phi\}_n \quad ,$$

is solved using Jacobi's method.[22] The terms ω_n^2 represent the natural frequencies squared, and the column vectors $\{\Phi\}_n$ represent the computed modes of vibration.

A detailed explanation of this three-dimensional computer code, including computer input and output information will soon be available from the Civil Engineering Department of Montana State University.

III-2.2 The Vibrational Characteristics of a Sphere Using Tetrahedral Elements.

The solid elastic sphere was chosen for a test problem, simply because the exact characteristic modes and frequencies can be derived.[25,26]

As a result of the simple geometry of the sphere, the characteristic modes appear in two distinct classes: C_1 modes where the dilations as well as the radial component of displacement are zero, and C_2 modes where the radial component of the curl of the displacement is zero. The zero displacement curl for C_2 modes indicates zero rotation about radial lines.

Numerical values for the characteristic modes and frequencies of the sphere are computed using the various tetrahedral assemblages shown in Figure 7. Figure 7(a) shows a crude 7-node assemblage composed of one node at the center and six nodes uniformly distributed around the spherical outer surface of unit radius. Figure 7(b) shows a 19-node assemblage having one node at the center and eighteen nodes distributed around the spherical outer surface. Figure 7(c) shows a somewhat more refined 33-node assemblage in which one node is located at the center, six nodes are uniformly distributed at the mid radius, $r=\frac{1}{2}$ (the mid radius nodes are distributed precisely as those of Figure 7(a), scaled down by a factor of two), and twenty-six nodes are distributed as shown around the spherical surface at r=1. Figure 7(d) shows the most refined assemblage of the four

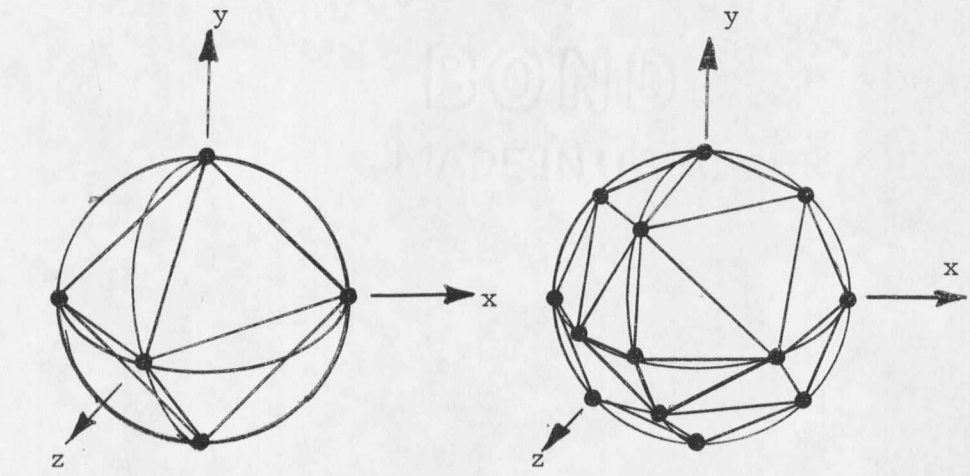

(a) 7-node assemblage
(a = .682)

(b) 19-node assemblage
(a = .889)

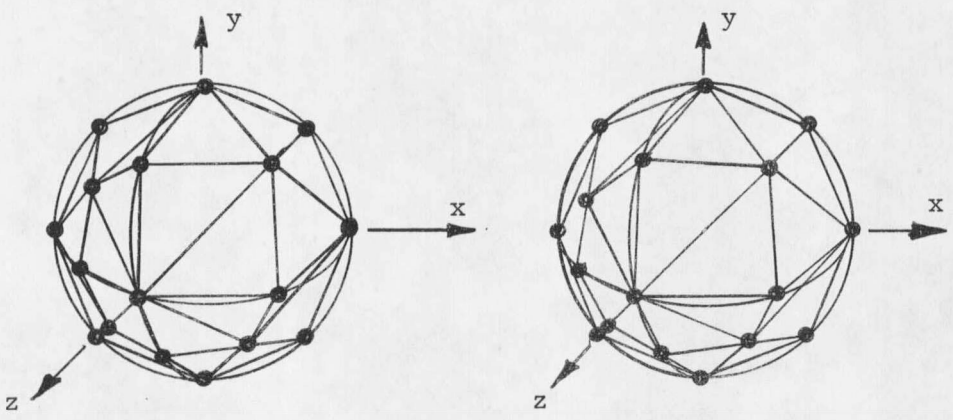

(c) 33-node assemblage
(a = .920)

(d) 59-node assemblage
(a = .920)

Figure 7. Assemblages of tetrahedral elements inscribed in a unit sphere. The effective radius, a, is defined such that the volume of the assemblage is equal to $4/3\pi a^3$.

pictured. This 59-node assemblage contains one node at the center, six nodes around the spherical surface r=1/3, twenty-six nodes around the spherical surface r=2/3, and twenty-six more nodes at r=1 as pictured. The twenty-six nodes at r=2/3 are radially in line with those at r=1.

The effective radius, a, of each assemblage is defined as the radius of the sphere having the same volume as the assemblage. The various effective radii are shown in Figure 7.

The numerically computed natural frequencies for the fundamental radial mode of the various assemblages of tetrahedrons are compared with the exact frequency in Figure 8. A general convergence trend is noted as the number of nodes in the assemblage of tetrahedral elements is increased, but it is noteworthy that the frequency computed for the 19-node assemblage is in error by an amount greater than the frequency of the 7-node assemblage. The fundamental radial frequency for the 59-node assemblage is just 2-1/3% above the exact frequency.

It is anticipated that in some future work more of the computed modes can be identified with exact modes so that their associated natural frequencies can be compared.

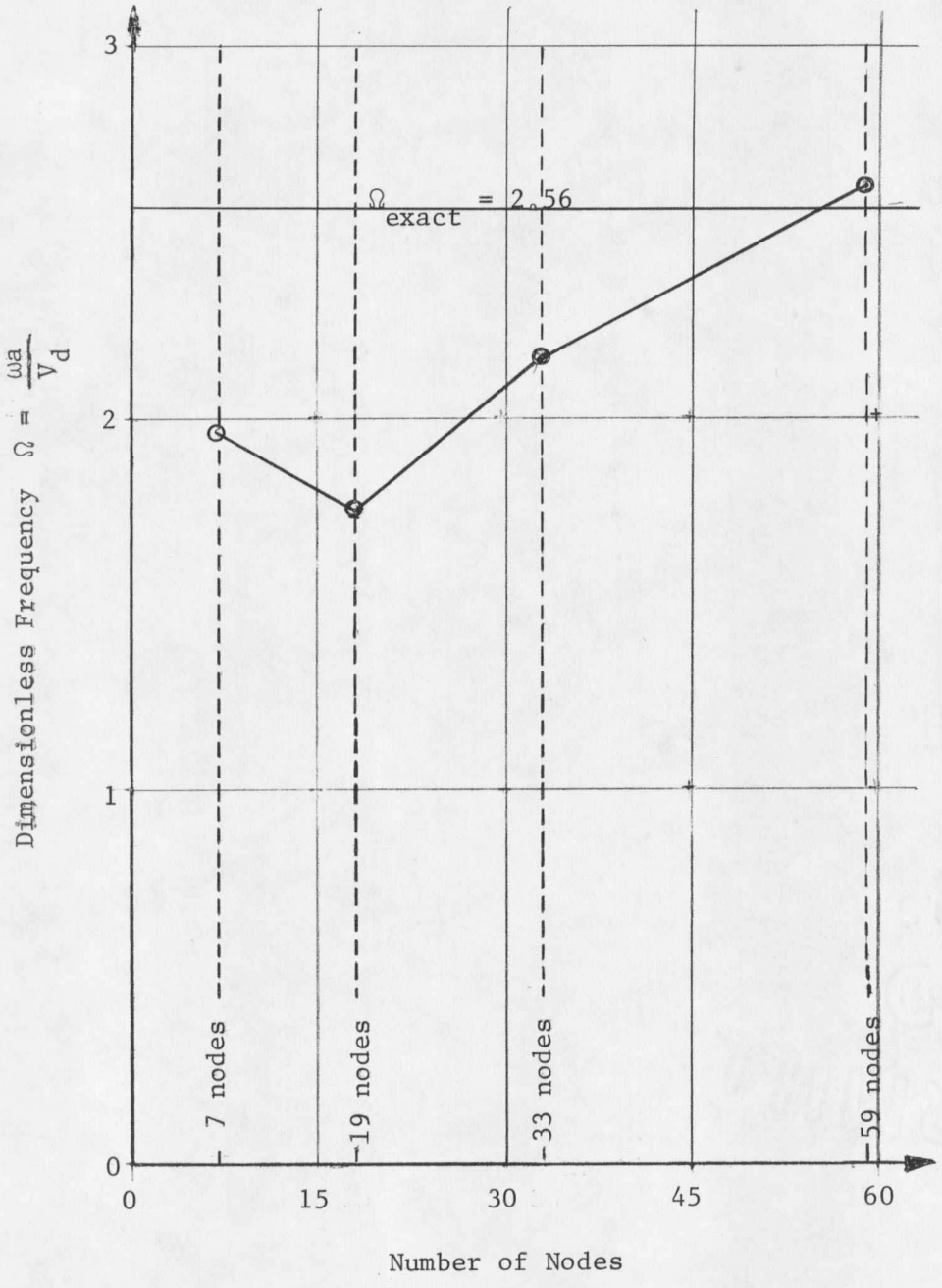

Figure 8. Numerically computed natural frequencies compared with the exact frequency for the fundamental radial mode of a sphere ($\nu = \frac{1}{4}$)

Chapter IV

CHARACTERISTIC FREQUENCIES AND MODES OF EARTH DAMS

IV-1 Three-Dimensional and Nonthree-Dimensional Methods

Previous attempts to compute characteristic frequencies and modes of the earth dam have been restricted to one- and two-dimensional behavior. The earth dam is, of course, a three-dimensional solid, capable of motions in all three directions. However, it appears that the nonthree-dimensional treatments can give realistic values for some of the vibrational characteristics of an earth dam. This fact is substantiated by vibrational tests performed on full-scale dams.[4,27] At the same time, these experimental studies indicate the need for a truly three-dimensional treatment of the dam to fully explain the observed behavior.

The two nonthree-dimensional representations of an earth dam appearing in the literature are the "shear-wedge" dam[6] and the "plane-strain" dam.[9]

The notion of the shear dam was originated in a paper by Mononobe, Takata, and Matumura[5] and later expanded upon by Ambraseys.[6] Due to the great thickness of an earth dam relative to its height, the resistance to motion in the upstream-downstream direction is primarily due to shear distortions. In this simplified approach, all points on the dam are restricted to horizontal motions in the upstream-downstream direction,

and relative motion of points along a horizontal straight line passing through the thickness of the dam is ignored.

Keightley[28] proposed to treat the shear-wedge dam numerically in order to permit irregular boundary geometry at the end abutments. Frazier acted on this proposal and computed some of the lower modes of vibration for Bouquet Canyon Dam.[4,7] Some of these results appear later in this chapter.

The plane-strain dam, first introduced by Ishizaki and Hatakeyama,[8] permits two components of motion, vertical and upstream-downstream motions. The assumption is made that the motions in the plane of a vertical cross-section transverse to the crest is the same for all such cross-sections, thus resulting in strains occurring exclusively in the plane of these transverse cross-sections. Due to the finite length of an actual dam, the motions in the transverse cross-sections will necessarily vary along the length; therefore, the plane-strain method is restricted to dams where the length is considerably greater than the height, and to those modes that consist of very long transverse standing waves with negligible motions along the length of the dam. This is to minimize variations in the displacement of lines parallel with the crest, thus approximating the plane-strain state.

There is some question regarding the value of the plane-strain analysis for treating a vibrating earth dam that is being excited by

motions of the abutments. The plane-strain dam does not provide for energy transfer from one transverse cross-section to the next; thus, it is strictly applicable only for a seismic disturbance occurring in the foundation that has no component of motion parallel to the length of the dam. Furthermore, the two nonzero components of motion -- vertical and upstream-downstream -- must act in such a way that all points along boundary lines drawn transverse to the axis of the canyon move exactly in phase. That is, the boundary motion must be independent of the location along the length of the dam. This is a particularly difficult requirement because the large length-to-height ratios required of the plane-strain dam enhance the possibility of phase changes in the foundation motions along the length of the dam.

While the shear-wedge dam may be better suited to treat variations in the upstream-downstream foundation motions along the length, no provision is made in the shear-wedge dam to treat variations in these foundation motions through the thickness. Also, the exclusion of the vertical motions makes the shear-wedge method undesirable for analyzing dams, because certain types of dam failures are certainly related to the vertical accelerations.

Certainly no nonthree-dimensional analysis can provide all the answers; therefore, a three-dimensional analysis is needed. The main difficulty here is the numerical problem of dealing with the extremely

large matrices that are generated from the discrete system. These computations can be unwieldy, even for the largest digital computers.

IV-2 Wedge-Shaped Dam in a Rectangular Canyon

IV-2.1 Shear-Wedge Analysis

The exact values for the characteristic modes and frequencies of the homogeneous shear-wedge dam in a rectangular canyon, pictured in Figure 9, are available.[6,7] The modes vary as trigonometric functions along the length and as Bessel functions over the height of the dam according to the relationship

$$w_{n,r}(x,y) = \left[Y_o(\beta_n H)\, J_o(\beta_n Y) - J_o(\beta_n H)\, Y_o(\beta_n y) \right] \cdot \sin \frac{r\pi x}{L} \quad \ldots\ldots \quad (63)$$

where n and r are integers that take on values from one to infinity. The height H, the length L, and the two coordinate axes x and y are all pictured in Figure 9. J_o and Y_o are zero order Bessel functions of the first and second types, respectively, and β_n are the zeros of the equation

$$-Y_o(\beta_n H)\, J_1(\beta_n h') + J_o(\beta_n h')\, Y_1(\beta h') = 0 \quad (64)$$

where h' is the height truncated from the crest as shown in Figure 9.

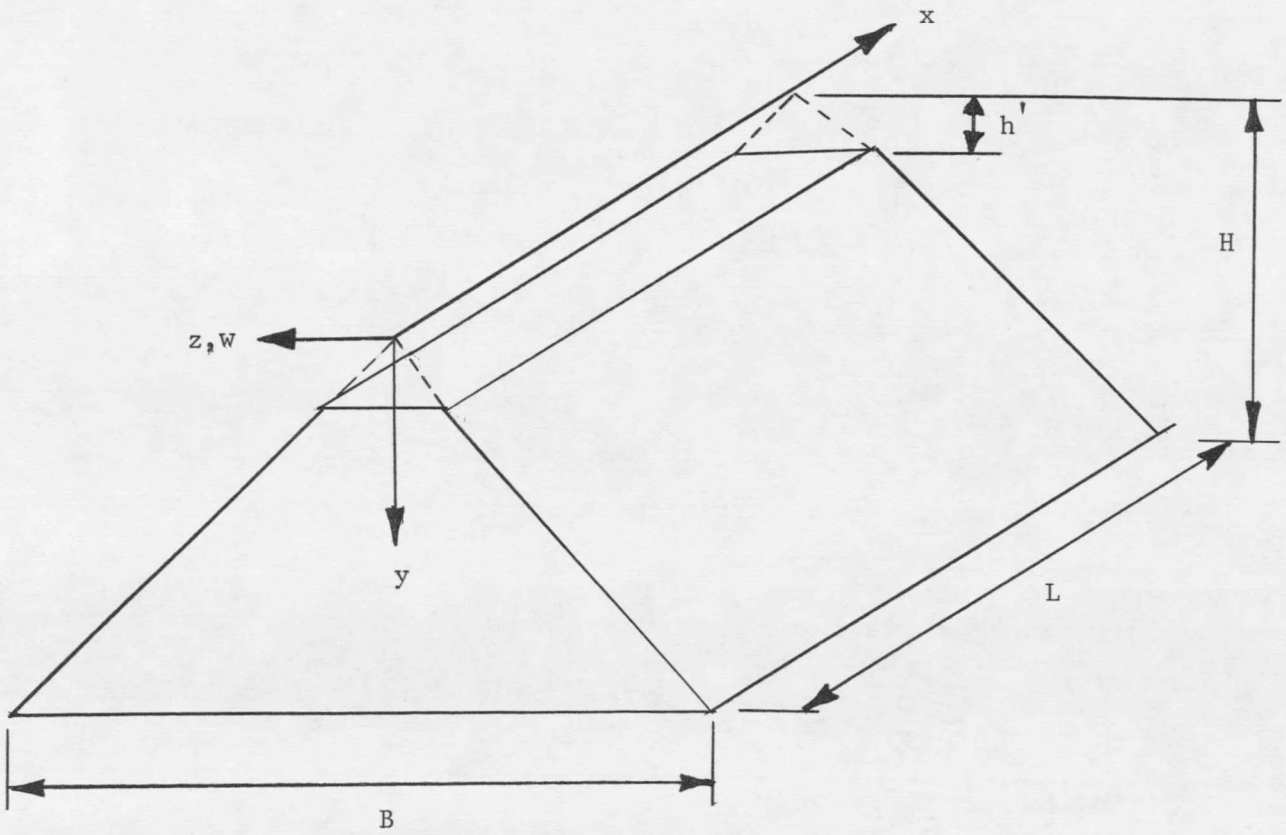

Figure 9. Truncated wedge-shaped dam in a rectangular canyon.

The exact value of the natural frequency associated with the (n,r) mode is

$$\omega_{nr} = V_s \left[\beta_n^2 + \left(\frac{r\,\pi}{L} \right)^2 \right]^{\frac{1}{2}} \tag{65}$$

where V_s is the shear wave velocity, which is assumed to be the same throughout the volume of the dam.

It is noted here that for a large length-to-height ratio, β_1 is much larger than π/L. In fact, ignoring the term π/L when calculating ω_{11} introduces only about 6% error for L/H = 4. This fact adds credibility to the plane-strain analysis of dams having large length-to-height ratios for computing ω_{n1} since L is taken as infinite in the plane-strain analysis, thereby eliminating the length dimension from the analysis. It is seen from Equation (65), however, that the greater the length-to-height ratio, the more closely spaced are the frequencies, ω_{1r}, r=1,2,3, ..., and therefore the greater the necessity of including these modes of vibration, which are missed in the plane-strain analysis, in response calculations. This is probably the fundamental weakness of the plane-strain analysis as it applies to an earth dam.

A numerical scheme for treating the shear-wedge dam is described elsewhere by Frazier.[7] Briefly, the displacements in the upstream-downstream direction are assumed to vary linearly between the nodes of the

grids pictured in Figure 10. This procedure corresponds with that of a low order finite-differencing scheme.

The natural frequencies computed by use of the two grids of Figure 10 are compared with the exact frequencies, given by Equation (65), in Table II. Here, the following parameters were used: H = 110 ft, h' = 30 ft, L = 100 ft, B = 220 ft, and V_s = 1000 ft/sec.

As might be expected, the more refined 90-node grid shows better agreement with the exact frequencies than the 16-node grid. It is also worth noting that the natural frequencies taken from the two discrete systems are below the corresponding exact frequencies, with better agreement at the lower frequencies.

IV-2.2 Plane-Strain Analysis

The characteristic frequencies and modes of the discrete plane-strain dam cross-section pictured in Figure 11(f) have been computed previously by Chopra and Clough.[9] The triangular section is 300 ft high and 900 ft wide at the base, with side slopes of 1½:1. The material is homogeneous, isotropic, and linearly elastic, with a shear wave velocity V_s = 1000 fps and a dilatational wave velocity V_d = 3316 fps, and a unit weight γ = 130 psf. These properties correspond to a Poisson's ratio ν = 0.45.

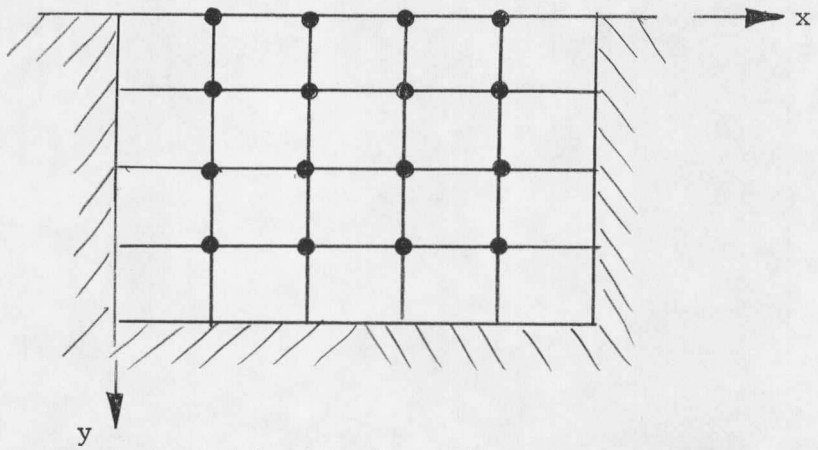

(a) 16-node grid

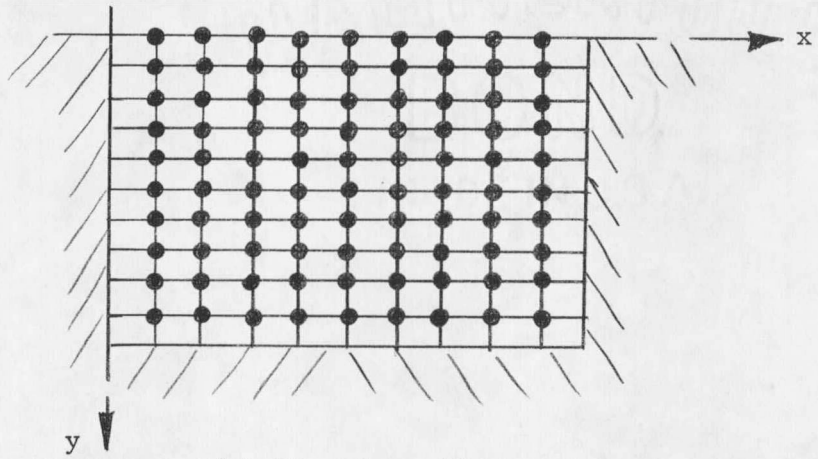

(b) 90-node grid

Figure 10. Upstream-downstream elevation view of a discrete approximation of a shear dam in a rectangular canyon.

Table II

Comparison of the Natural Frequencies Obtained Numerically with the Exact Frequencies for a Truncated Shear Dam in a Rectangular Canyon.

frequency designation	exact frequency	numerically obtained frequency			
		16-node grid		90-node grid	
ω_{nr}	(rad./sec)	frequency	% error	frequency	% error
ω_{11}	39.970	39.387	1.46	39.840	0.32
ω_{12}	67.517	63.650	5.73	66.543	1.44
ω_{21}	69.014	65.352	5.31	68.391	0.90
ω_{22}	87.885	82.286	6.37	86.707	1.34
ω_{13}	97.434	85.507	12.2		
ω_{31}	104.645	89.561	14.4		
ω_{23}	112.510	99.303	11.8		
ω_{32}	117.947	102.573	13.0		
ω_{14}	128.070	98.191	23.4		
ω_{33}	137.282	116.668	15.0		
ω_{24}	139.883	111.180	20.3		
ω_{41}	142.163	103.395	27.2	135.288	4.83
ω_{42}	152.221	114.850	24.5		
. . .	six natural frequencies have been omitted				
ω_{44}	187.123	;37.043	26.7	176.475	5.69

In order to study the effect that the element refinement has on the natural frequencies, all of the discrete representations pictured in Figure 11 are analyzed. The lowest three natural frequencies of each of the discrete representations are plotted and connected by solid lines in Figure 14 along with a sketch of each of the three corresponding mode shapes. From this solid-line plot it would appear that further refinements of the discrete system are not really necessary, since the computed natural frequencies vary only slightly with the more refined 36V-node and 55V-node assemblages.* The lowest five natural frequencies of the 15V-node assemblage are within 2.5% of the corresponding frequencies of the 55V-node assemblage.

Further investigation, however, casts some doubt on the degree of accuracy with which the refined assemblages of Figure 11 represent the actual continuum. For example, to study the effect that the element configuration has on computed natural frequencies, the triangular plane-strain dam section was represented by triangular elements oriented so that each element had one horizontal side, as pictured in Figure 12. The lowest three natural frequencies of each of these modified element configurations are plotted in Figure 14 using dashed lines. The three natural

---

*The letter "V" indicates that vertical lines are used in defining the sides of the triangular elements. Letter "H" will be used to designate elements which are bounded on one side by a horizontal line.

frequency convergence curves representing the "H" assemblages of Figure 12 are surprisingly far removed from the curves representing the "V" assemblages. Whereas, it would appear from observing the solid-line convergence curves alone that the lower few natural frequencies of the 15V-node assemblage are within 2.5% of the exact values (represented by the refined 55V-node assemblage), the lowest three natural frequencies of the refined 55H-node assemblage of Figure 12(e) vary from the corresponding frequencies obtained from the 55V-node assemblage of Figure 11(f) by 0.5%, 4.6%, and 7.0%, respectively. This indicates that, with the exception of the lowest natural frequency, not only are the natural frequencies of the 15V-node assemblage probably not within 2.5% of the exact frequencies, but the natural frequencies of the more refined 55V-node and the 55H-node may not even be within 2.5% of the exact frequencies.

This rather large spread in the two sets of convergence curves of Figure 14 gives rise to the following questions: Just how much does the element configuration affect the computed natural frequencies? Is it possible that a seemingly good element configuration could give extremely poor values of frequency?

In order to answer these questions the additional element configurations of Figure 13, each having about the same degree of refinement as the 15V-node and the 15H-node assemblages, were analyzed. The lowest three natural frequencies of these additional assemblages as well as the fre-

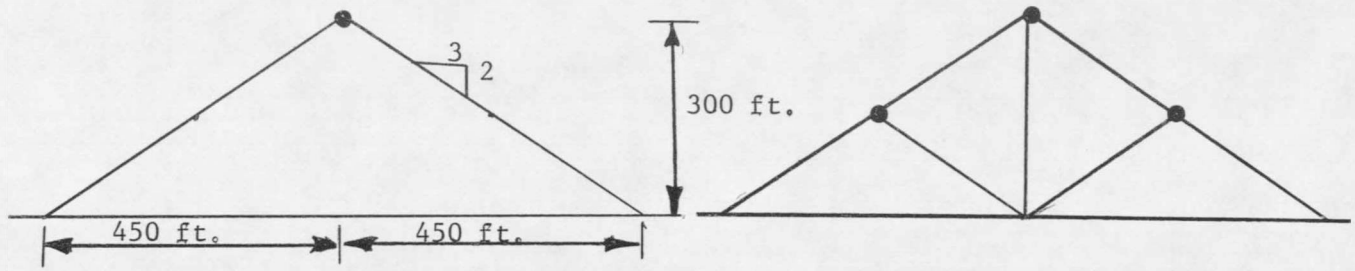

(a) 1-node assemblage

(b) 3V-node assemblage

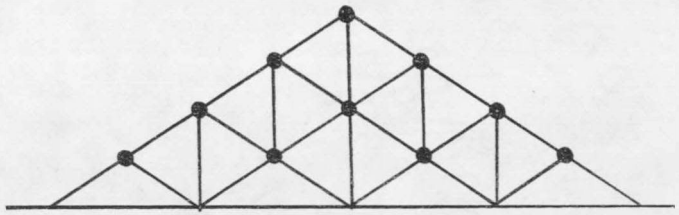

(c) 10V-node assemblage

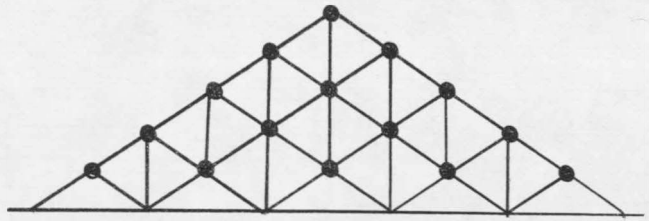

(d) 15V-node assemblage

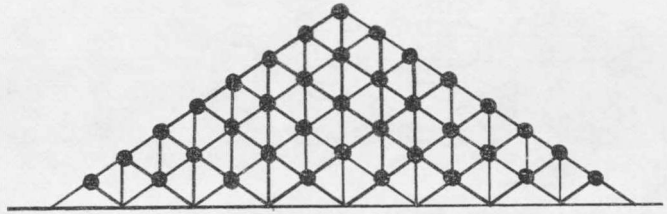

(e) 36V-node assemblage

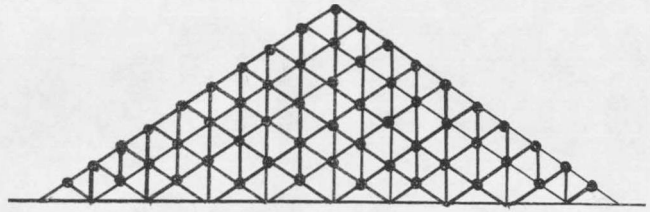

(f) 55V-node assemblage

Figure 11. Discrete representations of a plane-strain dam illustrating various degrees of refinement.